THE JOURNAL OF PHYSICAL CHEMISTRY B

Article

pubs.acs.org/JPCB

The Q-Cycle Mechanism of the bc_1 Complex: A Biologist's Perspective on Atomistic Studies

Antony R. Crofts,*[,†,‡] Stuart W. Rose,[‡] Rodney L. Burton,[†,⊥] Amit V. Desai,[§] Paul J. A. Kenis,[§] and Sergei A. Dikanov[∥]

[†]Department of Biochemistry, University of Illinois at Urbana−Champaign, 419 Roger Adams Lab, 600 South Mathews Avenue, Urbana, Illinois 61801, United States

[‡]Center for Biophysics and Quantitative Biology, University of Illinois at Urbana−Champaign, 179 Loomis, 1110 West Green Street, Urbana, Illinois 61801, United States

[§]Department of Chemical & Biomolecular Engineering, University of Illinois at Urbana−Champaign, 600 South Mathews Avenue, Urbana, Illinois 61801, United States

[∥]Department of Veterinary Clinical Medicine, University of Illinois at Urbana−Champaign, 1008 West Hazelwood Drive, Urbana, Illinois 61801, United States

Supporting Information

ABSTRACT: The Q-cycle mechanism of the bc_1 complex is now well enough understood to allow application of advanced computational approaches to the study of atomistic processes. In addition to the main features of the mechanism, these include control and gating of the bifurcated reaction at the Q_o-site, through which generation of damaging reactive oxygen species is minimized. We report a new molecular dynamics model of the *Rhodobacter sphaeroides* bc_1 complex implemented in a native membrane, and constructed so as to eliminate blemishes apparent in earlier *Rhodobacter* models. Unconstrained MD simulations after equilibration with ubiquinol and ubiquinone respectively at Q_o- and Q_i-sites show that substrate binding configurations at both sites are different in important details from earlier models. We also demonstrate a new Q_o-site intermediate, formed in the sub-ms time range, in which semiquinone remains complexed with the reduced iron sulfur protein. We discuss this, and a spring-loaded mechanism for modulating interactions of the iron sulfur protein with occupants of the Q_o-site, in the context of control and gating roles. Such atomistic features of the mechanism can usefully be explored through simulation, but we stress the importance of constraints from physical chemistry and biology, both in setting up a simulation and in interpreting results.

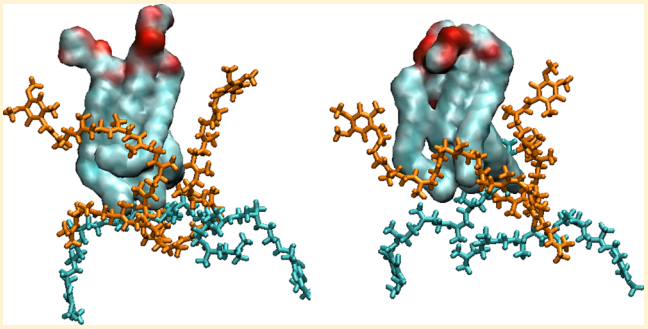

INTRODUCTION

The central role played by enzymes of the bc_1 complex family in the energy metabolism of the biosphere has been supported by half a century of progress summarized in the Q-cycle mechanism.[1−8] Crystallographic structures show that the complex in both mitochondria and bacteria is a homodimer, with a catalytic core of three subunits in each monomer, cytochrome (cyt) *b*, cyt c_1, and the Rieske iron−sulfur protein (ISP).[9−14] Each monomer has four metal centers, hemes b_H and b_L in cyt *b*, the 2Fe2S cluster in ISP, and heme c_1 in cyt c_1. In some bacterial complexes, no other subunits are structurally defined, but in *Rhodobacter sphaeroides*, the complex expressed under photosynthetic growth has an additional subunit IV of uncertain function.[15,16] Mitochondrial complexes have up to eight additional subunits. For some the function is known and for many it is uncertain,[9,12,17,18] but since none contain redox centers, or impinge on the catalytic sites, they are unlikely to be involved directly in the mechanism.

The interest of the Q-cycle (Figure 1) is that it doubles the energy saved from each photon compared to that if the ubiquinol (QH_2) generated in the photochemistry directly reduced the cytochrome (cyt) c_2 oxidized. Instead, QH_2 is oxidized in a bifurcated reaction at the ubiquinol oxidizing site (Q_o-site) that directs one electron via a high-potential chain, 2Fe2S cluster and heme c_1, to cyt c_2, leaving an intermediate semiquinone (SQ) at the Q_o-site (SQ_o). This is oxidized by a different, low-potential chain, hemes b_L and b_H, which delivers the electron to reduce ubiquinone (Q) at the quinone-reducing site (Q_i-site). Since this takes two electrons, the Q_o-site reaction must turn over twice, with the electron from the first stored as SQ_i, which is then reduced to QH_2 on the second turnover.

Special Issue: Klaus Schulten Memorial Issue

Received: October 18, 2016
Revised: February 26, 2017
Published: February 28, 2017

DOI: 10.1021/acs.jpcb.6b10524
J. Phys. Chem. B 2017, 121, 3701−3717

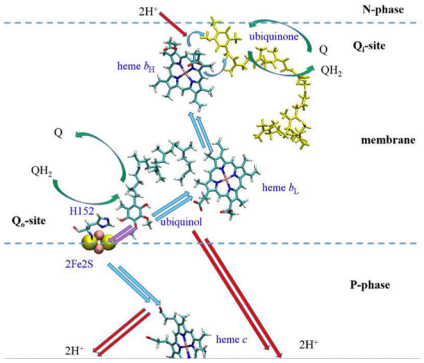

Formation of ES_1-complex

$$Eb_Hb_L \ldots ISP_{ox} + QH_2 \rightleftharpoons Eb_Hb_L.QH_2.ISP_{ox} \quad (1)$$

1^{st} e^- transfer (to high potential chain)

$$Eb_Hb_L.QH_2.ISP_{ox} \rightleftharpoons ISPH \ldots Eb_Hb_L.QH^{\cdot} \quad (2)$$

$$ISPH \ldots \text{heme } c^{+}{}_1 \rightleftharpoons ISP_{ox} \ldots \text{ferroheme } c_1 + H_P^+ \quad (3)$$

2^{nd} e^- transfer (to low potential chain)

$$Eb_Hb_L.QH^{\cdot} \rightleftharpoons Eb_Hb_L^- + Q + H_P^+ \quad (4)$$

$$Eb_Hb_L^- \rightleftharpoons Eb_H^-b_L \quad (5)$$

Q_i-site reaction

$$Eb_H^-b_L + Q + H_N^+ \rightleftharpoons Eb_Hb_LQ^{\cdot-}(H^+) \quad (6a) \text{ or}$$

$$Eb_H^-b_LQ^{\cdot-}(H^+) + H_N^+ \rightleftharpoons Eb_Hb_L + QH_2 \quad (6b)$$

Each of these main processes may involve several partial reactions, as represented in the kinetic model.

Figure 1. Consensus version of the Q-cycle. Left, the redox centers of a monomer of the *Rb. sphaeroides* bc_1 complex (taken from the MD). The reactions of the Q-cycle (equations to the right) are shown by magenta arrows (H-transfers), green arrows (Q, QH_2 exchange at catalytic sites), cyan arrows (electron transfers), and red arrows (H^+ transfers). QH_2 bound at the Q_o-site shows the ES complex of the bifurcated reaction. The mobile head of ISP provides the binding domain for the 2Fe2S cluster (space-filled lower left), the site of redox exchange. This moves from the position shown here (where the electron is transferred from QH_2 at the Q_o-site to ISP_{ox}) to H-bond with heme c_1 (where the ISPH is oxidized), an ~30 Å rotational displacement.

This QH_2 is recycled to replace one of those oxidized at the Q_o-site. Since protons are released on one side and taken up on the other, and electrons cross the insulating phase through the low-potential chain (Figure 1), the Q-cycle pumps $2H^+/QH_2$ oxidized across the membrane, with the following overall reaction:

$$QH_2 + 2\text{ferricyt } c_2 + 2H^+{}_N \rightleftharpoons Q + 2\text{ferrocyt } c_2 + 4H^+{}_P \quad (1)$$

Despite its "textbook" status, many features of the Q-cycle model remain controversial. The sites at which ubiquinone is reduced and oxidized involve four different proton-coupled electron transfer (PCET) reactions, in which the different properties of the semiquinone intermediate confer very different patterns of reaction. These are exploited both in the reaction mechanism and in control and gating functions. Our recent kinetic model for the reaction at the Q_o-site in the antimycin-inhibited complex includes kinetic and thermodynamic parameters for 14 partial processes, most of them determined directly using conventional physicochemical approaches.[4,6] The model takes account of existing thermodynamic constraints but is already under revision to include control processes revealed in recent work in two related areas.

First, collaboration with the Kaeberlein lab on understanding the longevity in *C. elegans* following mutation of ISP (strain *isp-1(qm150)*), and suppressor strains in the same subunit, has suggested a spring-loaded mechanism.[19,20] To understand why this is interesting, note in Figure 1 the large distance between the 2Fe2S cluster, to which the electron from QH_2 is transferred, and heme c_1, to which the electron is next delivered. Structures show that the ISP extrinsic domain containing the cluster can rotate on a tethering span to close the distance.[14,21,22] The spring-loading involves the counteraction of forces associated with formation of the enzyme–substrate (ES) complex, which pull on the tether span to extend a helical segment, and the forces trying to remake the helix. These involve additional partial processes, and their thermodynamic parameters need to be accommodated by redistribution of work terms among existing equilibrium constants. Longevity relates to a darker side of the enzyme—its production of reactive oxygen species (ROS)—which makes it an important player in the aging process.[2,19,20,23] The SQ_o intermediate can reduce O_2 to generate superoxide, the precursor of ROS, and much of the current interest lies in how the mechanism has evolved to minimize such processes.

The second new set of information relating to gating mechanisms comes from development in collaboration with the Kenis lab of a rapid mix/freeze quench apparatus based on a microfluidic mixer. The approach has allowed us to characterize an intermediate product of the QH_2 oxidation reaction, proposed to involve SQ_o in complex with the reduced ISP ($ISPH^{\bullet}$), a novel state with interesting properties.[24] These include spectroscopic features, the sub-ms kinetics, thermodynamic parameters, and incorporation into the kinetic scheme. High resolution EPR approaches should allow us to establish molecular parameters for the spin coupling that can be directly compared to outcomes from quantum chemical (QC) calculation.

In this paper, we review recent progress on understanding partial processes of the bc_1 complex mechanism at the atomistic level, discuss what remains to be achieved, and focus attention on those aspects of importance from the perspective of a biologist. In several recent studies, the interest has been in the application of state-of-the-art computational approaches and the biology has sometimes taken second place. These studies have arrived at important conclusions, but these might be suspect if the starting computational models have defects. The main impetus in developing a new model comes from this obvious starting point; modeling of mechanism through simulation is necessarily conjectural, and success in relating the outcome to the experimental base through which computation can be validated must depend on how realistic the model is.

The Role of Spring Loading in Control. The mutations in *C. elegans* above have focused attention on the role of ISP and movement of its extrinsic cluster binding domain in control and gating of ROS production. From previous work in bacterial systems,[25−29] the primary mutation in *isp-1(qm150)* (Pro-225 → Ser, in the cluster binding domain, equivalent to P146 (bovine), P166 (yeast), P136 (*Rb. sphaeroides*)) likely introduces distortion of structure at the surface of the cluster domain that interfaces with cyt *b*. This would result in a steric hindrance to impede formation of the enzyme–substrate (ES) complex, and hence limit ROS production. Then, the suppressor mutants (eight different point mutations in the tether) would relieve the inhibition. The fact that all of the

DOI: 10.1021/acs.jpcb.6b10524
J. Phys. Chem. B 2017, 121, 3701−3717

simulation suppressor mutations were in the same subunit as the primary lesion but were well-separated from that site in the sequence and in the structure. This localizes the underlying mechanisms for both longevity and its suppression to this subunit and the involvement of these specific regions. When the extrinsic head of ISP docks on cyt *b*, the driving force is associated with binding (predominantly, the H-bond between the occupant and His-152) and the protein interfaces involved. The work from binding contributes one set of the forces in the spring-loaded scenario. The other set of counteracting forces is associated with a change from helical to elongated chain in the tether span where the suppressor mutations are located; the binding force pulls on the tether to extend it. The loss of binding energy for formation of the ES complex from the primary mutation is likely overcome in the suppressor mutations by weakening the helical forces in the tether (Figure 2). Values of direct relevance to the spring-loaded scenario[19,20,25] have been estimated for both forces from studies of *Rhodobacter* mutants, though these were originally constructed to test the role of the tether in movement.[26−29] Complexes of reduced ISP (ISPH•) are formed with several different inhibitors, or with quinone (Q). In binding of ISPH• with different occupants, the paramagnetic property allows characterization of the interaction through changes in the EPR spectrum. Displacement of values for $E_{m,\ ISP}$ when ISPH• is pulled out of the equilibrium mix allows estimation of binding free energies,[21,22,30] which depend on occupant and vary with mutation. Simple thermodynamic considerations then provide values for changes in the counteracting forces, as detailed in the Supporting Information for ref 19, summarized in Figure 2. In the ES complex, ISP_{ox} is not paramagnetic, so this "handle" cannot be used, but binding information can be determined from similar displacements through kinetic characterization.[3,4,31,32] In considering the role of spring-loading, the critical point of interest is that the binding to form the ES complex involves similar counteracting forces, but on electron transfer to the intermediate products, ISPH• and SQ_o, these must dissociate for further progress. The force stored in the tether on extension of the "spring" when the ES complex is formed is available to drive the dissociation of ISPH• from SQ_o. This would favor the forward chemistry, minimize SQ_o occupancy, and thus help to explain protection against ROS production. However, the new SQ_o.ISPH• complex introduced above does not dissociate on a ms time scale, as would be necessary for rapid forward chemistry. The intermediate state is trapped, a feature of obvious interest to be discussed further below.

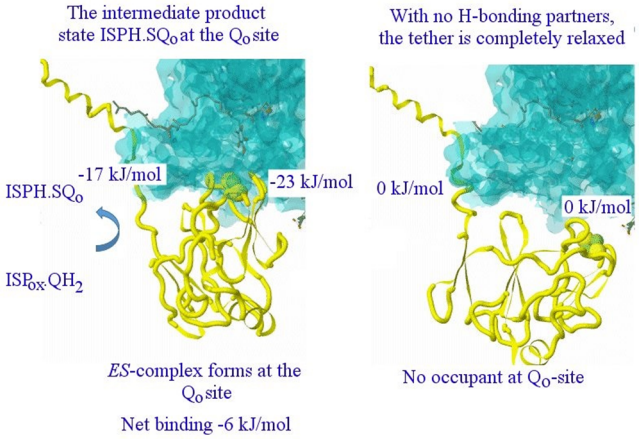

Figure 2. The ISP subunit from structures of mitochondrial bc_1 complexes showing conformations that change with the occupancy of the Q_o-site (adapted from refs 21, 22, 30, and 83). The structures show ISP with the fully extended tether (left) on binding at the Q_o-site (here with stigmatellin) and with the fully relaxed tether (right) when no bond is formed with a Q_o-site occupant. In the spring-loaded mechanism,[19,20,25] the experimentally determined binding free energy (~ −6 kJ/mol) is the difference between the work involved in binding (−23 kJ/mol) and the work needed to extend the tether (−17 kJ/mol), referred to the relaxed state (ΔG° = 0 for both). The values shown are estimated from work on ISP mutants in *Rb. capsulatus* and *Rb. sphaeroides*.[25−27,29] The curved arrow shows the first electron transfer reaction after formation of the ES complex. When SQ_o.ISPH• separates by spatial displacements to allow interaction with acceptors, the binding force is lost, and the energy stored in the extended spring is available to drive displacement.

Examples of Some Problems in Computational Simulation of the bc_1 Complex. Most molecular dynamics (MD) simulations start from the crystallographic structures. The atoms are frozen in a lattice constrained by contacts with neighboring components of the unit cell, and information on dynamic features is limited to the mobility shown by B-factors. For membrane proteins, the prison is even more unnatural. There is no membrane, but instead, ancillary lipids, detergent molecules, waters, etc., fill the interstices. The MD simulation is set up to liberate the native structure from this prison, an essential preliminary to mechanistic exploration. Crystallographic models of the bc_1 complex from vertebrate mitochondria or bacteria show a dimeric structure with a substantial empty volume in the dimer interface to the N-side of the closely packed protein interface between the b_L hemes. It is unlikely that this void represents a vacuum. In support of this, in higher resolution structures of the yeast mitochondrial complex, electron density in the site has been resolved, and specific phospholipids identified.[33] One cardiolipin molecule occupies the central cavity, and tails from other lipids contribute more peripherally.[33,34] The volume is defined by a protein scaffolding, symmetrical about the vertical axis of the dimer, consisting of transmembrane helices, and transverse (amphipathic) helices at the level of phospholipid head groups. The scaffolding restricts access at this level but allows access from the hydrophobic lipid phase. The former restriction might be expected to impede ready diffusion of phospholipid from the membrane into the volume. The scaffolding helices screen the two Q_i-site volumes from the "void", but substrate access is from a contiguous volume so that the quinone tails mingle with the lipids in the void. These features can be seen in our model, with the "void" volume now partly occupied by two phosphatidylglycerol (PG) molecules (Figure 3, Figure SI-1).

In two previous MD simulations of *Rhodobacter* complexes accessible to the authors, it was assumed that the problem of the void would be addressed by "the physics", as explored in MD simulation. In practice, the MD eliminated the void but in one case by partial collapse of the protein. Significantly, during 350 ns of simulation, although lipid tails explored and partly filled the volume, no phospholipid molecule diffused in. In another case, the void was filled by flooding with waters. Neither of these physical solutions is likely to be natural. In the former case, a partial unfolding from the crystallographic configuration of one of the transverse scaffolding helices occurred, which also disrupted the volume around one Q_i-site of the complex, precluding realistic simulations involving that

DOI: 10.1021/acs.jpcb.6b10524
J. Phys. Chem. B 2017, 121, 3701−3717

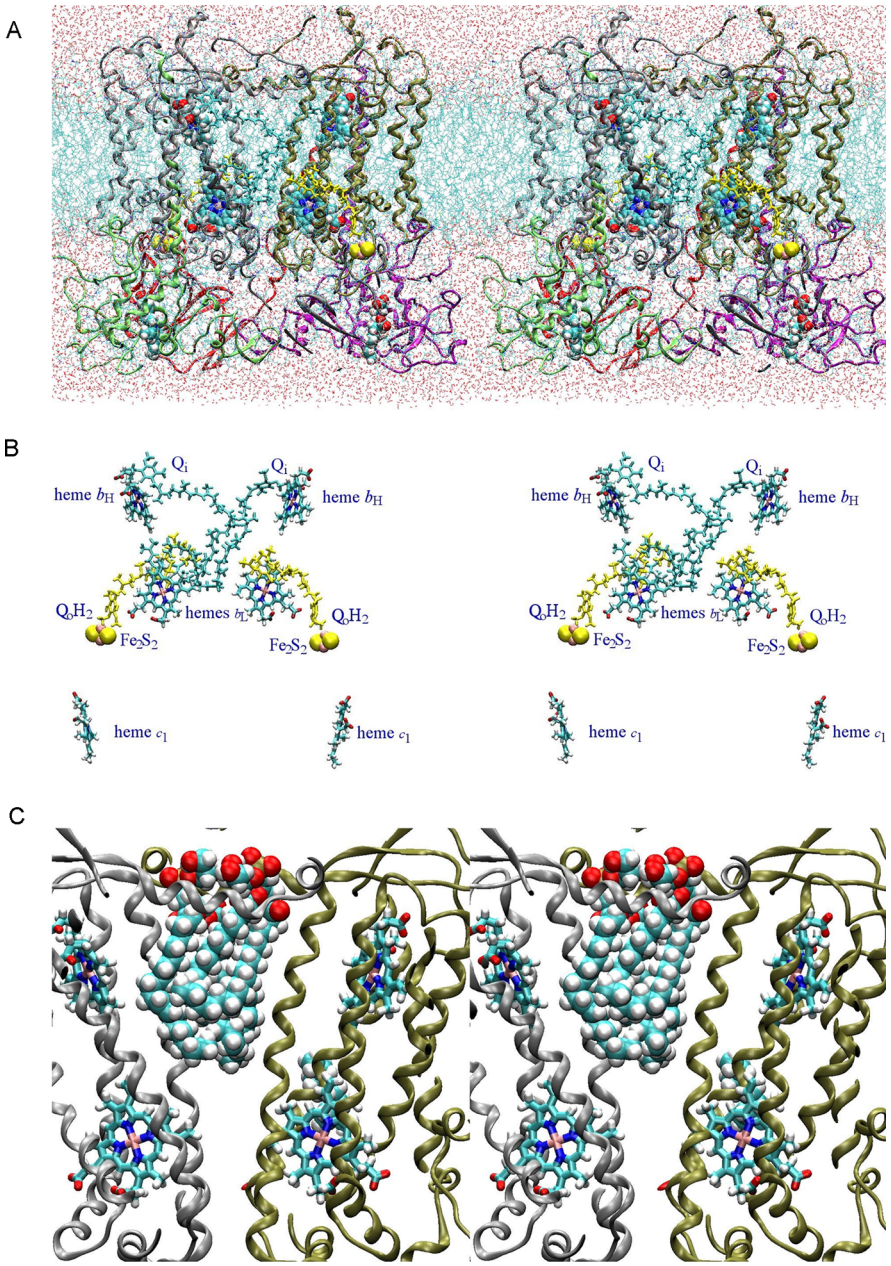

Figure 3. Cross section through the MD model of the *Rb. sphaeroides* bc_1 complex after 31 ns of a production run. (A) The initial occupants were replaced by parametrized molecules, with ubiquinone (Q_i) in the Q_i-site and ubiquinol (Q_oH_2) in the Q_o-site. A slice through the protein, shown as a cartoon, reveals the prosthetic groups colored by chain, embedded in the membrane between aqueous phases, with lipids and waters represented by lines for the bonds. The redox centers are shown by VDW spheres (for hemes and 2Fe2S-cluster) or by licorice bonds, colored as below. The "void" is the ∇-shaped space defined by a scaffold of membrane spanning and transverse amphipathic helices (center, top of protein), here occupied by lipid. (Stereo pair for crossed-eye viewing.) (B) The protein stripped away to show the redox centers, to facilitate identity: all redox groups except 2Fe2S are shown by licorice bonds, the hemes are in CPK colors; QH_2 at the Q_o-site is yellow; Q at the Q_i-site is cyan; the 2Fe2S cluster is shown by VDW spheres. (C) The same view of the protein but zoomed to highlight two lipids (PG, shown by van der Waals spheres) occupying the void, with the *b*-type hemes (licorice bonds, CPK colors) for reference, and the scaffolding helices, showing how exchange of phospholipids would be impeded at the headgroup level. Structure taken from the trajectory exploring formation of the ES complex, at a frame of ∼31 ns, when the bond to H152 had stabilized.

volume. In the latter, the waters would have introduced a high dielectric phase in a volume lined by hydrophobic residues suitable for lipid interactions. Because of the proximity of the Q_i-sites, occupation by waters would significantly change the physical chemistry of the site. However, the focus in both papers was the Q_o-site reaction, and since this is on the other side of the protein from the Q_i-site, it was supposed that disruption of structure at the latter would have little effect on the former. The problem of eliminating the void has been averted in simulations from the Róg group by introduction of a cardiolipin molecule to occupy the void,[35,36] effectively simulating in a *Rhodobacter capsulatus* bc_1 complex the yeast configuration.

A second set of problems lies in representation of the native membrane. Early MD simulations of the mitochondrial bc_1 complex had used a simple 1-palmitoyl-2-oleoyl-*sn*-glycero-3-

DOI: 10.1021/acs.jpcb.6b10524
J. Phys. Chem. B 2017, 121, 3701−3717

phosphocholine (POPC) membrane,[37] still preferred in a recent effort using a *Rhodobacter* complex.[38] A more natural membrane model was introduced by Postila et al.,[39] with a composition based on that of mitochondrial membranes, also adopted in our own recent simulation.[8] Unfortunately, in equilibrating the membrane model, forces came into play that converted the *cis* fatty acid side chains to the unnatural *trans* configuration, thereby substantially altering the membrane properties. Whether this was important or not to simulation of function is not clear. The *Rhodobacter* are versatile bacteria, like many others, and can adapt their membrane composition to cope with environmental stress. For example, under phosphate-limited growth, much of the phospholipid component of the *Rb. sphaeroides* membrane (though not cardiolipin or PG) was substituted by nonphosphorus glycolipids.[40] Strains can be engineered by mutation to eliminate synthesis of cardiolipin from PG (CL− strain[41]), and these conditions have been combined to explore the dependence of growth, expression of cytochromes, and activity of respiratory and photosynthetic chains on membrane composition. The tested parameters were not attenuated, even when the CL− strain was grown under phosphate limiting conditions.[40,41] The only phospholipid present under the latter conditions was PG, from which it is obvious that no other common phospholipid could be required. Although it is not obvious that modifications in lipid content would alter the protein behavior, a natural membrane is obviously preferable. Of special interest is the high ubiquinone content of the native membrane.[42−44] Any natural simulation should at least include this component, even though the second order processes involved in substrate or product binding are not readily accessible on the MD time scale.

It seems likely that the void is accounted for by disorder in lipids naturally incorporated on assembly of the complex which were not detected by X-ray diffraction. Indeed, as noted above, a more stable structure has been achieved in *Rb. capsulatus* models by populating the void with a cardiolipin,[35,36] as seen in the yeast complex. These and other possibilities are readily explored by simulation.

The Limitations of Conventional Approaches to Atomistic Understanding of Mechanism. In a complex mechanism like the Q-cycle, it is widely recognized that the parameters determined experimentally (rate and equilibrium constants, driving forces, reorganization energy, etc.) reflect interplay of many "invisible" partial processes at the atomistic level, even when a reaction can be well-defined by a chemical equation. For these processes, direct measurements are not available, so feasible parameters must be estimated within constraints from conventional measurements.[4,6] We have pioneered exploration of some of these atomistic features more quantitatively through previous collaborations with the Schulten group, applying MD and QC approaches to several different mechanistic problems using MD models based on mitochondrial or *Rhodobacter* bc_1 complexes.[4,8,37] Building on this experience, we here introduce a new MD model using the *Rb. sphaeroides* bc_1 complex, in which the protein environment has been modeled in a native membrane, including ubiquinone, and are currently running unconstrained MD simulations (production runs) to explore the mechanism at the atomistic level under XSEDE support, discussed below.

METHODS

Classical Molecular Dynamics Simulations. MD simulations are performed using NAMD,[45] a highly parallel, publicly available MD program, with demonstrated scalability on many platforms. Currently, the molecular systems presented here can be modeled for 10−15 ns/day when run at 2 ns/step on 400 STAMPEDE processors. Simulations involving lipids use the latest CHARMM36 force field in which the problem with consistency of lipid density has been resolved.[46] The simulations with proteins and prosthetic groups use the CHARMM36 force field with CMAP corrections,[47] supplemented by custom built topologies from collaborators. Water molecules are represented explicitly by the TIP3P model.[48] In all simulations, the temperature was maintained constant at 310 K using Langevin dynamics with a damping coefficient of 1 ps^{-1} and the pressure at 1 atm using the Langevin Nosé−Hoover method.[49,50] Long-range electrostatic forces will be calculated without truncating using the particle mesh Ewald (PME) method.[51] For all simulations, 2 fs will be used as the integration time step. Umbrella sampling (US)[52] with replica exchange molecular dynamics[53] will be used in some projects to calculate the potentials of mean force (PMF) associated with the studied processes. The weighted histogram analysis method (WHAM)[54−56] will be used to construct the PMF from the calculated trajectory files. All of these methods are standard and fully implemented in NAMD. Collaborations will allow us to extend the range to include application of more specialized approaches.

Rapid Mix/Freeze Quench Protocol. To poise bc_1 complex with heme b_H reduced and b_L oxidized, 11 μM bc_1 complex in a buffer of 50 mM 3-(*N*-morpholino)-propanesulfonic acid (MOPS) at pH 8.5, 100 mM KCl, with 0.1% dodecylmaltoside (DDM) and 10% glycerol (buffer A) was incubated in the presence of 65 μM 6-(10-hydroxydecyl)-2,3-dimethoxy-5-methyl-1,4-benzoquinone (OH-decylUQ, idebenone), 70 nM NDH-2 (NADH.ubiquinone reductase from *E. coli*), and saturating antimycin A. The mixture was flushed with argon for 2 h in a Thunberg cuvette before mixing with 0.5 mM NADH held in the bulb, and then allowed to incubate for 30 min. The redox state of the *b*-hemes and NADH was monitored spectrophotometrically. Heme b_H became reduced with a lag on reduction of the Q-pool ($t_{1/2} \sim 6$ min), but somewhat remarkably, heme b_L remained oxidized (at least out to 90 min), despite the strongly reducing conditions provided by the excess NADH ($E_h \sim -350$ mV). In a separate anaerobic chamber, 800 μM equine ferricyt *c* in buffer A was flushed with argon to keep it anaerobic. Other mixtures could be used to explore different starting states. The two mixtures were transferred to the reaction syringes under strictly anaerobic conditions before mixing to start the reaction.

The reaction progress was assayed using a rapid-mix, freeze-quenching approach.[57−59] An ultrafast microfluidic mixer was used to rapidly mix the reactants and eject the mixed solution in the form of a jet onto supercooled rotating copper wheels to quench the reaction within ~30 μs. The Z-shaped mixing channel was designed to enable sub-millisecond mixing,[60] and the operating conditions were optimized (on the basis of the physics of fluid mechanics and surface tension) to eject the mixed solution in a jet as opposed to droplets. A myoglobin/sodium azide reaction was used to calibrate our apparatus as in Appleyard et al.,[61] calibrated to an instrumental dead time of ~30 μs, similar to the 50 μs observed in ref 60.

RESULTS AND DISCUSSION

The Bifurcated Reaction at the Q_o-Site. The finer features of control and gating cannot be appreciated without

DOI: 10.1021/acs.jpcb.6b10524
J. Phys. Chem. B 2017, 121, 3701−3717

some deeper insights into the Q-cycle mechanism through which the complex operates (Figure 1). Our current picture for the Q_o-site reaction involves mobile dancers (ISP extrinsic domain, SQ_o, several side chain rotations) in a molecular ballet of reactions linked to the chemistry, driven by overall work terms well characterized by conventional approaches. However, the ballet is choreographed by atomistic forces. Recent evidence suggests that, at the Q_o-site, control and gating of the first electron transfer involves the spring-loaded mechanism mentioned above,[19,20] while that of the second electron transfer involves Coulombic couplings that come into play as H^+ and electron separate on oxidation of SQ_o (initially formed as the neutral SQ ($QH^\bullet$) by heme b_L). Such Coulombic effects are complex, especially so when electrostatic forces from the neighboring protein and solvent perturb electronic orbitals, and *vice versa*. Additional complexity is introduced by equilibration between dimers. Kinetic data suggest that electron transfer across the dimer interface (between the b_L hemes) does not contribute a significant fraction of the normal forward flux,[3,62,63] but certainly, Coulombic effects and slow electronic equilibration can occur.[3,64] To explore such systems requires application of several different areas of physicochemical expertise, and the field has recently attracted such diverse interest.

The Rate Limiting Process. The first electron transfer at the Q_o-site is rate-limiting overall,[1,4,32] with the rate constant determined by the unique properties of the proton-coupled electron transfer mechanism, which can be summarized in the following Marcus–Brønsted form:

$$\log_{10} k = 13 - \frac{\beta}{2.303}(R - 3.6) - \gamma\frac{(\Delta G^\circ_{ET} + \lambda_{ET})^2}{\lambda_{ET}} - (pK_{QH_2} - pK_{app}) \quad (2)$$

Here $\beta/2.303$ is the slope of dependence of $\log_{10} k$ on electron transfer distance[65] with β = 1.4 Å^{-1}, γ is $F/(4 \times 2.303RT)$ = 4.23 in this treatment,[66] and λ_{ET} is the Marcus reorganization energy for the electron transfer component. The terms to the right can be seen as $\log_{10}$ probabilities whittling away the limiting rate constant ($k \sim 10^{13}$ s^{-1} at bond vibrational rates). The observed rate constant is $k \sim 10^3$ s^{-1}, but models based on structures suggested that the distance for electron transfer is ~7 Å, for which the expected value would be very much faster (~10^8 s^{-1} using typical values for reorganization energy, $\lambda \sim 0.7$ V). The rate constant is lowered from the value expected for simple electron transfer (the Marcus value, the first three terms on the right in eq 2) by the improbability of finding the proton in the favorable position along the H-bond through which both electrons and protons are transferred (the rightmost Brønsted term). This explanation for the rate constant discrepancy came from clues provided by structures. Although none of them have shown a quinone species in the catalytic site, structures with some types of inhibitor (stigmatellin, 5-*n*-undecyl-6-hydroxy-4,7-dioxobenzothiazole (UHDBT)) all showed specific H-bonding from a ring >C═O (or >C═O$^-$) to $ISPH^\bullet$, involving one of the histidine ligands to the 2Fe2S cluster (His-152 in *Rb. sphaeroides*). With $pK_{red} \sim 12.5$, this side chain is protonated at physiological pH, and would serve as a H-bond donor. Since the inhibitors were thought of as quinone analogues, it was natural to suggest a similar pattern for binding of ubiquinone, involving $ISPH^\bullet$ and one of the redox active >C═O groups of the quinone ring in the g_x = 1.800 complex.[21] Extrapolating from this to the quinol form then provided an obvious model for the ES complex. However, this involves QH_2 and the oxidized ISP (ISP_{ox}), for which the polarity would demand that the ring >C—OH acted as a donor to the H-bond to N_ε of the dissociated H152 of ISP_{ox}[22,67,68] ($pK_{ox1} \sim 7.6$). This configuration provides an obvious pathway for both proton and electron transfer, through the H-bond, to histidine and the cluster, respectively. A second clue then came from the redox chemistry of ISP, which showed that, over the physiological range, the E_m value varied with pH, indicating that reduction involved both an electron and a proton.[7,68−71] We suggested that the changes in pK_{ox1} in the physiological range seen on redox titration of mutant strains, and reflected in the pH dependence of electron transfer,[72,73] could be well explained as resulting from the changes in p*K*s of the two histidine ligands (H131 and H152 in *Rb. sphaeroides*) to Fe2 of the cluster.[1,69,71] This hypothesis has now been validated by direct measurement by NMR spectroscopy on the *Thermus thermophilus* ISP.[74] A third clue came from work in the Nocera group[75] on the rate of electron transfer between H-bonded partners in a model system, in which the groups involved (a diamine on one side H-bonded to a carboxylate on the other) could be exchanged without much effect on the photochemically generated driving force. Surprisingly, the observed rate in aprotic solutions was strongly dependent on the donor–acceptor configuration of the H-bond through which the electron and proton had to pass. They recognized that the proton-coupled electron transfer depended on the difference between the p*K* values of the groups forming the H-bond, which defined a Brønsted term specifying the probability that the H^+ would be favorably situated for electron transfer. By combining these hints, we could propose not only a simple model for the ES complex but also a simple explanation for the pH dependence of electron transfer in the physiological range, and the simple explanation for why the reaction was so slow, summarized in eq 2 and discussed extensively elsewhere.[1,32,69,73]

Previous Computational Studies. In the recent collaborative work[8] with the Schulten and Solov'yov groups, we have used molecular dynamics, supplemented by snapshots of critical states treated through QC calculation to examine the ES complex of the bifurcated reaction in the bc_1 complex from *Rb. capsulatus*. Modeling by MD simulation suggested a novel configuration, consistent with previously unexplained outcomes of mutagenesis studies of the key residue, Tyr-147,[76] and in marked contrast to the direct participation of E295 previously expected.[77] In subsequent studies,[78−80] polar residues contributing to binding of QH_2 and the 2Fe2S cluster were approximated through density function theory (DFT) to provide a QM model in which QC calculations were used to explore this state. In extending these calculations to an investigation of the first electron transfer, they used an approach based on the intrinsic reaction coordinate to explore potential pathways to product states, starting with different protonation states of H156 (equivalent to H152 in *Rb. sphaeroides*).[78] Although configurations with His-156 either protonated or not can be represented by competent QC models, only the complex in which ISP_{ox} has His-156 initially dissociated at N_ε provided a productive forward chemistry.[78] Several other recent papers[8,38,39,77] have included QC calculations of the first step of the bifurcated reaction at the Q_o-site. This is rate limiting under substrate saturation, and therefore of special mechanistic interest. Critical to the reaction profile is the configuration of the ES complex; conclusions about the PCET reactions involved depended on the model

DOI: 10.1021/acs.jpcb.6b10524
J. Phys. Chem. B 2017, 121, 3701−3717

chosen. In all models, the ES complex involved QH_2 in the site, H-bonded to the same histidine of ISP_{ox} docked at its interface with cyt *b*. In Martin et al.,[38] the electron transfer was treated in a somewhat truncated QC model, with parallel studies of the dielectric response of the protein and environment. In determination of the latter, the reaction was considered as starting with $QH^-.ISPH^{+\bullet}$, unencumbered by the Brønsted term, and treated as if the proton transfer was separate, so that the electron was transferred with full Coulombic consequence. However, the reaction is intrinsically neutral: $QH_2.ISP_{ox} \rightleftharpoons QH^\bullet + ISPH^\bullet$. In the PCET mechanism above,[1,7,32,69,71,81] with the ES complex formed with QH_2 H-bonded with N_ε of His-152 of ISP_{ox} dissociated ($pK_{ox1} \sim 7.6$ in the isolated protein[70]), formation of the complex (and hence the rate of reaction) depends on pH, as shown by the strong correlation between change in pK_{app} for electron transfer rate and change in pK_{ox1} in ISP mutant strains.[7,8] Since the ⩾C−OH of QH_2 (with $pK \sim 11.5$) donates the H atom to the H-bond, electrons and protons would follow the same path on oxidation by ISP_{ox}. Most of dielectric response needed would then be accommodated by electronic redistribution in the cluster and its ligands (as seen in the pK change of the histidines on reduction[7,69−71,82]). In the model considered by Postila et al.,[39] the electron transfer also occurred though the H-bond to histidine (H156 in *Rb. capsulatus*, H152 in *Rb. sphaeroides*) but with the histidine N_ε initially protonated, so that the histidine was not able to serve as a proton acceptor. Release of the proton therefore had to involve the other quinol ⩾C−OH, and a pathway, separate from that of the electron, via a bound water molecule, to which they assigned a key role. The MD model used by Barragan et al.[8] was initially parametrized following that of Postila et al.[39] but then was adapted so as to allow a testing of the Crofts et al. model,[1,7,32,69,71,81] with the histidine N_ε initially dissociated.

This simulation revealed unexpected features of the ES complex configuration, already noted above. Previous guesses based on the binding of stigmatellin had assumed that Glu-295 would provide a H-bond to the ⩾C−OH of the quinol distal from ISP. Since E295 mutations had a profound effect on function, a critical role had been assumed as acceptor for the second H^+, released on oxidation of the intermediate SQ_o. This was reinforced by the striking rotational displacement of E295, seen in structures with myxothiazol (or *E*-*β*-methoxyacrylate (MOA) type inhibitors), that both opened a volume for diffusion of SQ_o and brought the carboxylate group into contact with a water chain to the aqueous exterior, thus providing a pathway for proton release.[21,83] Barragan et al.[8] found instead that Tyr-147 spontaneously rotated from the position in the stigmatellin structure to serve the H-bonding function to QH_2. In their new model, Y147 also H-bonded to E295, and this allowed it to serve a relay function with the glutamate, so that the latter could still act as a proton acceptor. Reinterpretation of results from earlier literature on mutations at this residue,[76] and our recent detailed analysis[6] of additional mutations at Glu-295, seemed to provide support for this novel configuration. In Y147F,[76] in which the H-bonding potential was lost, the apparent K_m determined from the dependence of the rate of QH_2 oxidation on the degree of reduction of the Q pool indicated a substantially reduced affinity for the Q_o-site, consistent with a binding function in the native strain. On the other hand, the small increase in K_m on mutation of E295 to D or G observed in earlier studies,[83] confirmed in later work, was found to be spread to either side of the wild-type value in other strains when additional mutants were included, suggesting that Glu-295 had little if any effect on binding of QH_2.[6] In addition, at least one structure (PDB ID 1sqv) has been published in which the equivalent tyrosine (Y131 in beef) H-bonds to the inhibitor UHDBT at the Q_o-site.[10] This arrangement has been discussed in detail by Berry et al.[9] They were also able to identify such a configuration in electron densities for some of their own UHDBT-occupied structures. These results are of obvious importance in supporting the new configuration.

QC Simulations of the First Electron Transfer. Both the ES complex and its transition through the first electron transfer have recently been simulated in MD/QC calculations in a continuation of our collaboration with the Schulten and Solov'yov laboratories.[8,78] The outcomes of these calculations show a gratifying agreement with the mechanism suggested above but with a new wealth of atomistic detail. Free-energy profiles of the reaction coordinate from ref 78 are similar to that expected from eq 2, including energy levels, and endergonic nature. In the physicochemical profile (Figure 4), the

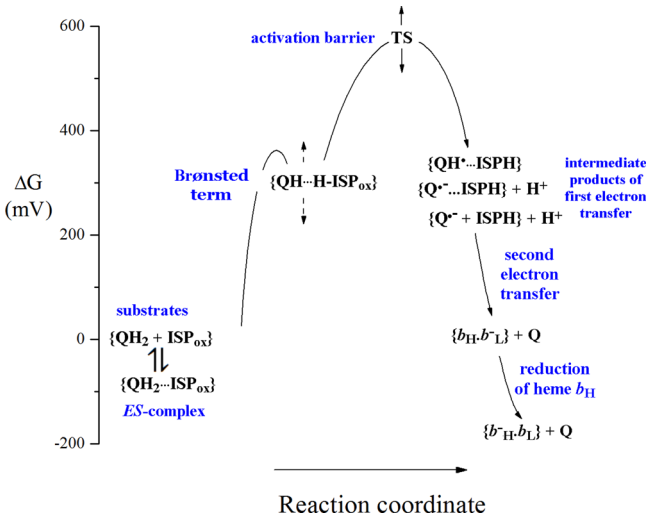

Figure 4. Marcus−Brønsted reaction profile of the Q_o-site reaction (updated from refs 1 and 7). Values for ΔG are calculated from experimental data. The vertical dotted arrows show limits on estimated values. The reaction follows the path expected from the Marcus−Brønsted treatment. The profile is similar to that generated by QC simulation in Barragan et al.,[78] set up with the ES complex ($ISP\cdots QH_2$) as the starting state, in which QH_2 is the H^+ donor to H152 N_ε in the H-bond, so that the reaction would be expected to follow the same path as that from the Marcus−Brønsted approach.

contribution of the Brønsted barrier is shown as a distinct state, but in the equivalent linear form of eq 2, the last two terms would represent the product of probabilities, and, with the rapid rate constants for H^+ transfer in H-bonds,[84] would therefore behave as a composite term. The approach through a QM superposition of states simulates not only the profile but also this composite feature, in the landscape from QC calculations.[78]

In an interesting investigation of the diffusion of O_2 into the Q_o-site, and its reduction to generate super oxide, Husen and Solov'yov[80] have also extended the model from ref 8 to approximate the product state in which the first electron transfer has generated $Q^{\bullet-}.ISPH^\bullet$. In another extension, Barragan et al.[78] have explored the QC trajectory between ES

DOI: 10.1021/acs.jpcb.6b10524
J. Phys. Chem. B 2017, 121, 3701−3717

complex and this product state. We will discuss these models later in the context of new insights from the SQ_o.ISPH$^\bullet$ state introduced above. Two additional recent papers have considered the role of cardiolipin in stabilizing the structure,[36] and in facilitating delivery of protons to the Q_i-site mechanism,[35] also discussed later.

A New MD Model Using the *Rb. sphaeroides* bc_1 Complex. Biochemical approaches can validate (or otherwise) quantum calculations, and insights from quantum chemistry can guide mutational and spectroscopic efforts. For the new model discussed above, the bc_1 complex from *Rb. sphaeroides* has been embedded in a native membrane with the physiological complement of lipids, including ubiquinone, to fit the computational model better to the experimental reality. In designing this model, we have taken note of the two problems introduced above: (1) the void in crystallographic structures (Figure 3) and (2) the non-native membrane used in previous work. Since interpretations of the outcome in these previous simulations might have been distorted by these architectural blemishes, an important preliminary task has been to test alternative scenarios for dealing with the void. We have stabilized the complex by insertion of two phospholipid molecules (PG in Figure 3c), simulating what might be expected on population of the void from the membrane on assembly of the complex. The Róg group has shown in their simulation of the *Rb. capsulatus* complex[35,36] a similar improvement in stability when cardiolipin occupies the void. We chose two PG instead of the cardiolipin because function of the bc_1 complex in *Rb. sphaeroides* does not require cardiolipin (see below). These are important improvements, because they minimize structural displacements of protein or water in response to the void. No population of the hydrophobic volume by waters occurred in the model containing the two lipids. As already noted, although the POPC membranes of earlier models have been replaced by more natural ones, for example, the composition of the mitochondrial membrane,[8,39] in setting up these models, the membrane was relaxed by procedures that allowed the natural *cis* fatty acid side chains to isomerize to the unnatural *trans* form. In our present model, we have used the published composition (including ubiquinone) of the *Rb. sphaeroides* chromatophore membrane determined under conditions of growth similar to our own,[85] to implement a more natural simulation environment, and taken care to avoid artificial isomerization.

Preliminary simulations after relaxation of the model with all constraints removed (short runs ∼5 ns) showed that all three phases (protein, lipid, and water) behaved naturally. In longer trajectories, free diffusion of lipids was observed in the bulk membrane; diffusion of phospholipids was limited to 2D within the constraints of the polar heads, but ubiquinone and ubiquinol also explored the lipid phase through 3D excursion, except when bound at the catalytic sites. The two PGs placed in the initially void volume were retained for at least 125 ns. The behavior in the membrane will allow direct estimation of diffusion coefficients over the time course of a trajectory (to be discussed elsewhere). Water chains previously observed crystallographically were populated by waters, but these exchanged rapidly with the bulk. No waters were found in the "void" volume, except at the headgroup/water interface. These results provide some confidence that modifications to correct previous defects have been effectively implemented. Both the overall structure and layout of the Q_o- and Q_i-sites retained configurations close to those seen in the starting model (occupied in the initial crystallographic model (PDB ID 2qjy) respectively by stigmatellin and ubiquinone), when occupied by UQ_i respectively, in reduced or oxidized form at Q_o- and Q_i-sites (Figure 3) (this redox poise would be appropriate to the pool initially 90% oxidized). The stable configuration of the Q_i-site confirms that in ref 35, in which features of the Q_i-site mechanism were simulated in a *Rb. capsulatus* model of the bc_1 complex with cardiolipin in the void. However, our initial unconstrained production run, exploring a continuous trajectory of ∼125 ns, revealed significant differences from those previously reported in configuration of reaction complexes at both sites (Figures 3 and Figure *SI*-1). The basis of these differences obviously needs to be resolved.

In the Barragan et al.[78] complex leading to productive forward chemistry, three H-bonds stabilized the quinol: from H156 N_ε to QH_2 −OH (O2), from Y147 −OH to QH_2 −OH (O5), and from Y147 −OH to E295 $-COO^-$. In our simulations, these three residues were all found to participate in H-bond pairings of the Barragan et al. model, suggesting that drastic revision of previous work might not be necessary. Figure 5 shows (in part A) the state of the Q_o-site in frame 153 of the trajectory (at ∼30 ns), in which important H-bonds are highlighted, and (in part B) the distances for the H-bonds above, read from the trajectory as it evolves. In the time course shown, ISP_{ox} and QH_2 are initially separate, but over the first 90 frames (18 ns), the H-bond from QH_2 −OH to ISP_{ox} N_ε of H152 forms, dissociates, and then reforms and stabilizes the ES complex. During the entire trajectory, Y147, E295, and N279 explore configurations in which Y147 rarely visits QH_2. Mostly, E295 is busy swapping its association between the other two residues. However, no configuration in which all three H-bonds were simultaneously engaged (which formed the basis of their QC calculations) has yet been reached in our simulation. This volume of the protein also includes several exchangeable waters which are involved in H-bonding with the polar residues, and connecting to the heme b_L propionates and Arg-94, likely providing H^+ conducting pathways, including one to the P-phase water. Over the remaining time captured in this trajectory, Y147 occasionally (about only 10% of the time; see time course in part B) H-bonds with QH_2, as shown in part A. In the frame captured in part A, the two primary H-bonds to QH_2 stabilizing the ES complex (from H152 and Y147) are both present, but E295 is distant. In a continuation of this run, with the sampling interval decreased to 1 fs, the pattern persists at longer times (currently to ∼125 ns). If this pattern is confirmed in additional runs, it would require at least a modest change in interpretation of the previous result, that the release of a H^+ from QH$^\bullet$ involves collisional exchange with Y147, E295, and N279 via stochastic H-bonding, rather than the direct relay previously suggested.[78] The Barragan et al. model[78] included Y147 and E295 in the QC calculation, and they found that, without E295 included, the forward chemistry was thwarted. This may capture an important feature of the mechanism. The same role could be implemented in the stochastic mechanism above but, unfortunately, not in a self-contained QC calculation. On the positive side, a smaller model, omitting Y147 and E295, would be more tractable in QC calculations. More difficult to implement would be QC evolution along the reaction profile using snapshots, interrupted by MD simulation allowing equilibration with the stochastic possibilities from structural dynamics.

More extensive revision could be justified; it is possible that the earlier modeling[21,22,30,83] of the ES complex as involving

DOI: 10.1021/acs.jpcb.6b10524
J. Phys. Chem. B 2017, 121, 3701−3717

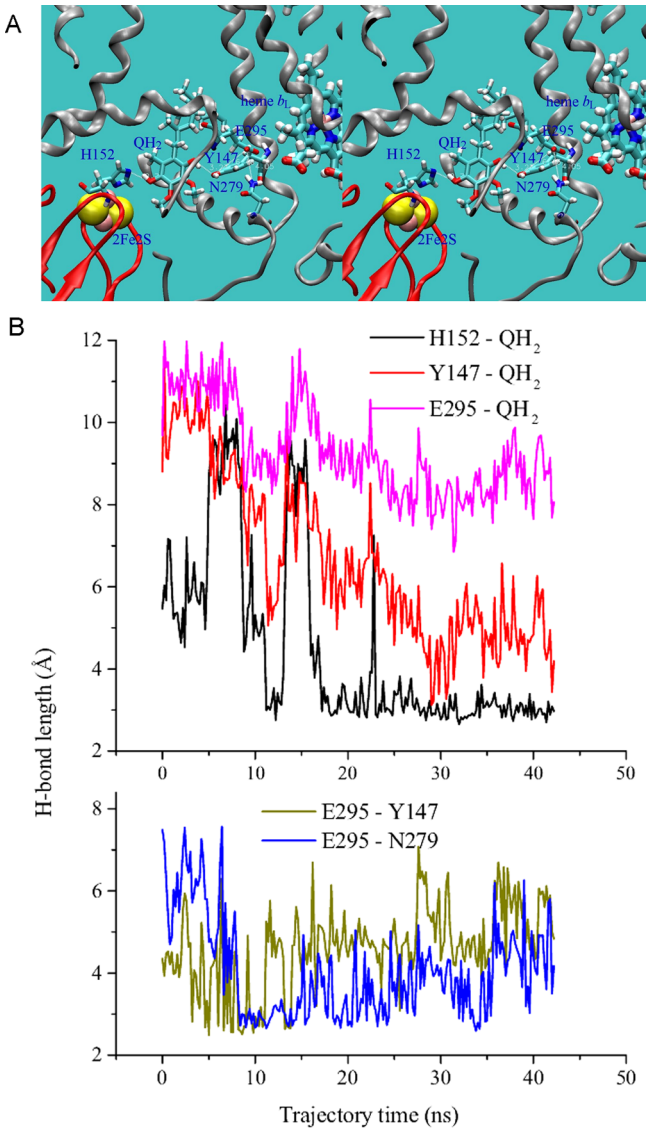

Figure 5. Formation of the ES complex. (A) The configuration of the ES complex after stabilization (at 31 ns). The bond to His-152 (at the left of the image) is stable after ~18 ns, and over the remaining time simulated, the bond from QH_2 to Tyr-147 (center) forms about 10% of the time. Throughout the trajectory, Glu-295 (right) remains too far from QH_2 to form a H-bond. (Stereo pair for crossed-eye viewing.) (B) Time course of stabilization. Details of the trajectory stabilizing the ES complex, as seen in the distance between non-H atoms of potential H-bonding groups. Bond distances are as follows: H152–QH_2 shows His-152 Nε to QH_2 O2; Y147–QH_2 shows Tyr-147 OH to QH_2 O5; E295–QH_2 shows Glu-295 OE1 to QH_2 O5; E295–Y147 shows Glu-295 OE1 to Tyr-147 OH; E295–N279 shows Glu-295 OE1 to Asn-279 ND2. The changes in H152–QH_2 distance reflect predominantly excursions of QH_2 out of the site, and therefore provide information on diffusional kinetics in the entrance channel.

E295 as a direct ligand to QH_2 has biased thinking toward an emphasis on a direct role in H^+ release. If so, an alternative scenario in which the product state $QH^{\bullet}$.$ISPH^{\bullet}$ dissociates to release the neutral SQ to diffuse in the site needs to be considered. E295 would then be involved only in transfer of the H^+ to the heme propionate after the $QH^{\bullet}$ is close enough to transfer the electron, thus facilitating an electrostatically linked PCET. The stochastic proton exchanges among this group of residues would enable transfers fast enough to make these last two models indistinguishable experimentally from the earlier model. Possible scenarios are discussed further below. One consideration in deciding between these scenarios is the need to constrain the SQ in the Q_o-site. Preference might depend on a simple physical principle; the low probability (high energy cost) of solvating a charged species favors mechanisms involving $Q^{\bullet-}$ as the liberated form, rather than $QH^{\bullet}$, since the former would have a much lower probability of escape into the lipid phase via the hydrophobic entrance channel.

In parallel, we have also run a preliminary simulation with antimycin occupying the Q_i-site, a commonly used experimental situation, since it allows ready measurement of turnover of the Q_o-site through reduction of heme b_H. The measured rate of QH_2 oxidation (in the first turnover) when heme b_H is initially oxidized is the same in the absence or presence of antimycin.[5,86] In line with this, the configuration of the ES complex examined followed essentially the same pattern as that in the absence of inhibitor (not shown).

Control and Gating in the Oxidation of SQ_o. The need for control/gating of the reaction was first noted explicitly by Oscyzka et al.,[87] who pointed out that, if rate constants for electron transfer were determined by distance, similar values would apply to oxidation of SQ_o in forward chemistry, and bypass reactions involving reduction of SQ_o by heme b_L, if both reactions occurred from the location at which it was generated from QH_2. Consequently, the bypass reactions, and those associated with ROS production, could occur at rates comparable to the normal forward reaction. To account for the observed slow rates, the reaction would have to be gated. Quite how this happens is under debate.

Although turnover is constrained by the limiting process, it is widely recognized that the second electron transfer must occur with a rate constant intrinsically much more rapid than the first. In normal forward chemistry, intermediate product states of the Q_o-site reaction must have a low occupancy (<0.02 per monomer, as judged by the <20 μs lag phase before the rate of reduction of heme b_H reaches its maximal value).[1,4,6,73,88,89] These states include SQ_o (in all forms) and ferroheme b_L. The rate constant for electron transfer to heme b_L in strains with E295 (the proton acceptor group) mutated to glutamine, lysine, or tryptophan can be directly determined because occupancies of both reactants, ferriheme b_L and SQ_o, can be measured. The rate is so slow that the heme remains oxidized over the time scale in which SQ_o becomes maximally populated.[6] Calculation of rate constant from measurement of ferriheme b_L and SQ_o occupancy in E295W then showed a value of $k_f \sim 10^3\ s^{-1}$. If this rate constant applied in normal forward chemistry, the occupancy calculated above would be much too low to explain the observed rate. The highest occupancy measured, under conditions of high driving force, was ~0.01, but under normal forward chemistry, a much lower value would be expected. Consideration of other scenarios is constrained by similar limitations on possible mechanisms. As proposed earlier, electron transfer to heme b_L could be increased 10^3-fold by migration of SQ to shorten the distance,[1,73,83] and this seems an economic explanation for the rates observed in the forward reaction.

In normal forward chemistry, the acceptor heme b_L is maintained in the oxidized form by electron transfer through heme b_H and the Q_i-site to reduce Q_o and under these circumstances, electron transfer is so rapid that no SQ_o accumulates.[24,57] Because the first step is endoergic, the back reaction is more rapid than the forward, and the second step

DOI: 10.1021/acs.jpcb.6b10524
J. Phys. Chem. B 2017, 121, 3701−3717

must compete with that. Many parameters enter into this competitive scenario, as explored by Hong et al.[73] Under any scenario for the forward reaction, the intermediate complex must dissociate rapidly into ISPH• and SQ_o. However, this depends on a coordinated set of processes. The tethered extrinsic domain of ISPH• must leave the association with the Q_o-site, and move close to heme c_1 to facilitate the subsequent transfer of the first electron. The SQ remains associated with the Q_o-site but, from the above, must move to initiate the second electron transfer of the bifurcation. All of these events—dissociation of the SQ_o.ISPH• state, electron transfer from SQ_o to ferroheme b_L, displacements of ISP and SQ_o—occur over a time scale of a few μs. On the other hand, if heme b_L is reduced, either initially or on turnover in the presence of antimycin, the SQ_o.ISPH• accumulates. Under these conditions, the complex turns over at ~1% of the uninhibited rate through bypass reactions, including generation of ROS if O_2 is present. In all earlier reports, the EPR properties of the SQ_o species reported showed no complexities in the spectrum, and no detectable association with H-bonding partners, suggesting that a loose binding might allow movement in the site. This is in contrast with the new SQ_o.ISPH• complex now to be discussed.

A New Intermediate SQ_o.ISPH• Trapped by Rapid-Mix/Freeze Quench. An important new set of data has been provided from our more recent work exploring kinetics of SQ_o accumulation. The microfluidic mix/freeze-quench approach for preparation of samples for EPR developed in collaboration with the Kenis lab has made it possible to measure of kinetics of formation of SQ_o in the sub-ms range, revealing a new intermediate SQ_o.ISPH• state (Figure 6). The fate of intermediate states depends on the availability of acceptors for the electron and the proton. Under conditions in which heme b_L was initially oxidized, no SQ_o signal was detected, indicating that the rate of oxidation was much greater than the rate of formation. This result confirms earlier kinetic studies,[57] although in that report, the failure to detect SQ was attributed to a concerted mechanism in which no intermediate state occurred. Turnover leads to formation of the newly identified state only when heme b_L has become reduced, either by redox poising prior to mixing with substrates or by preliminary turnovers of the Q_o-site when electrons are prevented from leaving the low potential chain. The features of interest are the kinetics of formation and a novel electronic structure, which shows new lines in the CW spectrum, changed saturation, and interaction through H-bonding to a neighboring N atom revealed through ESEEM experiments. We interpret these properties as showing that SQ_o is still in the H-bonded complex with His-152 (in *Rb. sphaeroides*) of ISPH•. In the forward chemistry, the SQ_o.ISPH• intermediate dissociates rapidly, perhaps aided by the spring-loading, but when heme b_L is reduced, it does not. What forces are in play under these conditions?

The features above show a new state, trapped by rapid freezing to liquid N_2 temperatures, in which SQ_o is associated with a neighboring paramagnetic center. SQ_o accumulates only as heme b_L becomes reduced, so neither oxidized *b*-heme is likely to be the spin partner. Although the *c*-hemes were likely oxidized, both would be quite distant, and all of the heme species have peaks far removed from this range (cf. ref 57). Since only ISPH• has a peak (at g_z = 2.02) in the region of the new SQ_o species, it seems likely that this is both the H-bonding and local spin partner. This is revealed through the appearance of additional lines, including a broad line at g = 2.06

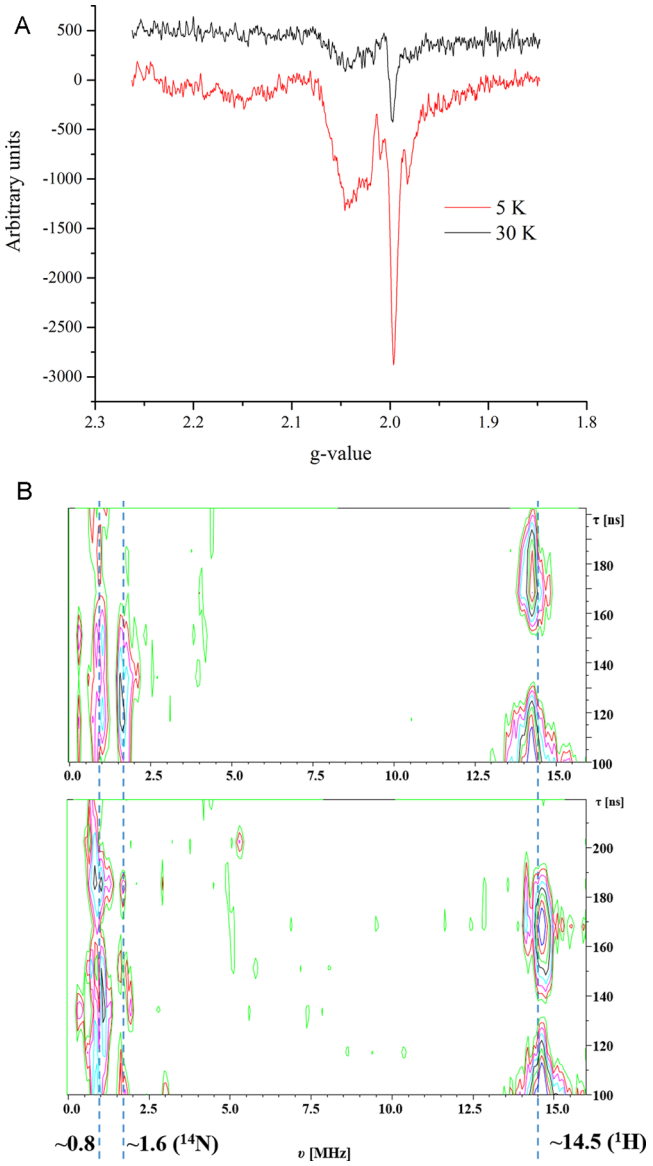

Figure 6. Semiquinone intermediate formed on turnover of the Q_o-site with heme b_H initially reduced. (A) CW X-band EPR spectra of a sample trapped early in the accumulation of SQ (at 280 μs after mixing), as heme b_L, initially oxidized, became reduced by turnover when heme b_H was initially reduced. The shape of the signal shows that the normal symmetrical narrow line shape of the SQ signal is distorted by electron spin−spin interaction with a neighboring paramagnetic metal center. The temperature dependence determined at 5 and 30 K (the 30 K trace at the top is offset by 500 units for clarity) shows that this substantially enhances the spin relaxation. The interaction is also seen in power saturation studies, and in the temperature and time dependence of field-sweep spectra (not shown). (B) The ESEEM spectra are presented as two-dimensional contours of the set of three-pulse ESEEM spectra of the bc_1 complex (sampled 4 ms after mixing), collected at g = 2.06 (top) and g = 2.005 (bottom). The spectra show contour plots of frequencies, υ (from the modulus of Fourier transform as time T increases), at different times, τ, using a three-pulse sequence $\pi/2...\tau...\pi/2...T...\pi/2...\tau...$echo. The initial time, τ, was 100 ns and was increased by 16 ns in successive traces. The lines at ~1.6 and 0.8 MHz in the spectra are from ^{14}N, and likely produced by interaction with a histidine nitrogen. The ^{1}H line in these spectra (at ~14.5 MHz) is produced by protons. The periodical variations of line intensity are due to dependence on time τ at stable frequencies. For both samples, the microwave frequency was 9.633 GHz and the temperature was 15 K. The magnetic field was 334.1 mT (top) and

DOI: 10.1021/acs.jpcb.6b10524
J. Phys. Chem. B 2017, 121, 3701−3717

Figure 6. continued

343.2 mT (bottom). The spectra show small differences in temperature sensitivity and different kinetics of decay, but nuclear spin interactions for ^{14}N, likely through H-bonding, were at the same frequencies (~1.6 and 0.8 MHz), and thus were likely with the same N atom. These values are consistent with the pure nuclear quadrupole frequencies of the protonated nitrogen in an imidazole residue, and suggest that the spin−spin interaction involves N_ε of His-152 of ISPH$^\bullet$, the same N atom as involved in the H-bond stabilizing the ES complex. This set of characteristics is very different from those of the dissociated SQ determined in earlier work.[6,23,111]

(dominated by ISPH$^\bullet$), seen in the CW spectrum (left) and in field-sweep three-pulse ESE spectra (not shown). Both temperature dependence (Figure 6, top) and saturation effects (to be published elsewhere), also obvious in field-sweep three-pulse ESE spectra, show enhanced relaxation expected from interaction with a metallic center.

Further details are revealed by pulsed EPR (Figure 6, bottom). The stacked plots show three-pulse ESEEM spectra in the frequency domain (MHz, bottom scale) at different times τ (z-axis, right-hand scale in ns), starting at zero = 100 ns and advancing by 16 ns from front to back. The data were measured at the g = 2.005 and g = 2.06 peaks of the CW EPR spectrum, the former dominated by SQ_o, the latter by ISPH$^\bullet$. Two spin interactions with ^{14}N are observed with frequencies of ~1.6 and 0.8 MHz but with differential evolution in τ. ESEEM spectra taken at g = 2.005 and at g = 2.06 report the same frequencies but small differences in temperature sensitivity and different kinetics of decay. The ESEEM frequencies (lines at ~1.6 and 0.8 MHz) are consistent with pure nuclear quadrupole frequencies of protonated N_ε (cf. ref 90). Since ESEEM spectra at the two g values show the same ^{14}N frequencies, they were likely with the same N atom, most probably that from N_ε of His-152 of ISPH$^\bullet$. The ESEEM spectra also showed a line at ~15 MHz from ^{1}H, which suggests that the interaction with N_ε of His-152 of ISPH$^\bullet$ involves a H-bond, as would be expected from its involvement in the H-bond stabilizing the ES complex from which the SQ_o state is formed in the first electron transfer.

An additional feature of interest is that the signal amplitudes are considerably higher than expected from an $S = {}^1/_2$ free radical, due to spin sharing with a neighboring center. A likely candidate, consistent with the configuration above, is the $S = {}^5/_2$ spin of the nearest Fe atom (FE2) of the cluster, to give a mean of S = 3, leading to significant amplitude gain. The amplification means that high-resolution pulsed-EPR techniques can be applied even with the state at low occupancy. Unfortunately, without a deeper understanding of the quantum chemistry of the superposition of states involved, a more complete quantification of the spin amplitude is not possible. However, this should certainly be tractable in QC calculations planned for the future.

How Does the New Complex Fit into the Forward Chemistry? The papers by Barragan et al.[8,80] exploit the important ES complex model, with QH_2.ISP_{ox} in association with Y147 and E295. Although this complex may be subject to revision, it remains an excellent starting point for exploring the role of these residues in release of the H^+. Any revision of the model must provide the basis for QC calculations of the reaction profile for the first electron transfer, and provide a reliable guide to intermediate product states. The initial intermediate product of the first electron transfer must involve a semiquinone that remains bound at the site. This is likely QH$^\bullet$.ISPH$^\bullet$, but in normal forward chemistry, that state is expected to rapidly dissociate to $Q^{\bullet-}$ and H^+ (or QH$^\bullet$), and ISPH$^\bullet$, free to separate, to reach the respective acceptors. The more recent studies from the Schulten/Solov'yov collaboration[78,80] have involved dissociation of the H^+ to give $Q^{\bullet-}$.ISPH$^\bullet$ as a transitional state which remains in association. However, the lifetime of intermediate states is uncertain in the time range explored in these calculations, and direct experimental evidence provides constraints only at much longer times. What different scenarios discussed need to be considered? Three possibilities are summarized in the following schemes:

Barragan, Solov'yov, Schulten mechanism:

heme b_L...QH_2.ISP_{ox}.E295 → heme b_L...QH$^\bullet$.ISPH$^\bullet$.E295

heme b_L...QH$^\bullet$.ISPH$^\bullet$.E295

↔ heme b_L...$Q^{\bullet-}$.ISPH$^\bullet$.E295(H^+)

heme b_L...$Q^{\bullet-}$.ISPH$^\bullet$.E295(H^+)

↔ heme b_L...$Q_o{}^{\bullet-}$...ISPH$^\bullet$

→ heme $b^-{}_L$(H^+)...ISPH$^\bullet$ + Q_o + E295

This paper:

heme b_L...QH_2.ISP_{ox}....E295

→ heme b_L...QH$^\bullet$.ISPH$^\bullet$....E295

heme b_L...QH$^\bullet$.ISPH$^\bullet$....E295

↔ heme b_L...$Q^{\bullet-}$.ISPH$^\bullet$....E295(H^+)

heme b_L...$Q_o{}^{\bullet-}$...ISPH$^\bullet$ + E295(H^+)

→ heme $b^-{}_L$(H^+)...ISPH$^\bullet$ + Q_o + E295

or

heme b_L...QH_2.ISP_{ox} → heme b_L...QH$^\bullet$.ISPH$^\bullet$

heme b_L...QH$^\bullet$.ISPH$^\bullet$ ↔ heme b_L...Q_oH$^\bullet$...ISPH$^\bullet$

heme b_L...Q_oH$^\bullet$...ISPH$^\bullet$

→ (E295-mediated)

→ heme $b^-{}_L$(H^+)...ISPH$^\bullet$ + Q_o

Barragan et al.[78] observed no dissociation of the $Q^{\bullet-}$.ISPH$^\bullet$.E295(H^+) state in the 350 ns of their trajectory, so the partial processes in the third line of the first reaction scheme are conjectural. The authors emphasize that, although dissociation of ISPH$^\bullet$ had not occurred on that time scale, this might be unremarkable in view of the ms range of experimental turnover. The experimentally determined lag in the kinetics of heme b_H reduction limits SQ_o occupancy to <0.02 in forward chemistry, making it very likely that dissociation and movement of SQ_o occur in the <10 μs range. In our kinetic model, $\tau \sim 10^{-7}$ s is needed. One additional point to note is that the spring-loaded effect noted above would favor dissociation.[19,20] This work-term, and its mechanistic expression, can be explored by the physics of the MD simulation if properly implemented, an obvious target for future studies. If the SQ_o.ISPH$^\bullet$ complex

DOI: 10.1021/acs.jpcb.6b10524
J. Phys. Chem. B 2017, 121, 3701−3717

is produced immediately after electron transfer from the ES complex of Figure 3, its lifetime in forward chemistry is much shorter than under the conditions in which we detect it. This state is formed only when the electron from SQ has nowhere to go, because the acceptor, heme b_L, is reduced. The proton would also have nowhere to go if E295(H^+) had been unable to pass on its H^+ during the previous turnover. Either or both could prevent SQ_o oxidation.

The reaction conditions under which the SQ_o.ISPH$^\bullet$ complex accumulates are similar to those present in the ischemic condition, a physiological state arising when tissues go anaerobic because the blood supply is interrupted (for example, in stroke or heart attack). The critical pathology comes into play during recovery, when oxygen is introduced to restart the bioenergetic pathways, and generates damaging ROS. Turnover of the bc_1 complex starts as oxidizing equivalents arrive via cyt *c*, and initiate the Q_o-site reaction with the *b*-hemes reduced, essentially the state in which SQ_o is generated in our experiments. It is also worth noting in the context of ROS production that, if the new state is indeed QH$^\bullet$.ISPH$^\bullet$, then the properties of the SQ species will be different from the free $Q^{\bullet-}$ state characterized in earlier experiments. To bring the spring-loading contributions into the picture, we note that, since both intermediate states evolve from the same ES complex, the same counterforces are initially in play. When the complex dissociates in forward chemistry, the binding force is lost, but in the new complex, a binding force must still be in play. This will affect the redox properties of both SQ_o and ISPH$^\bullet$. The reaction of SQ_o with O_2 is strongly dependent on the E_m values of the two couples involved; a change in $E_{m,SQ/QH_2}$ might reduce the rate so that ROS production is substantially reduced. In addition to a less favorable E_m value, the kinetic constraint from association with the ISPH$^\bullet$ will also provide an impediment. Perhaps these effects could account for the slower rate of O_2 reduction observed compared with that calculated.[80] Sarewicz et al.[64,91] have demonstrated an O_2-insensitive state with some properties in similarity, discussed in the Supporting Information. In our own experiments, the jet formed after mixing, in which the reaction evolves, is exposed to the open air, allowing a similar conclusion, that the state is O_2-insensitive.

At present, some features of the mechanism proposed and the properties required are hypothetical but could be constrained in the light of parameters from MD/QC simulation. The exciting prospect is that this important state can be simulated in a quantum mechanical model derived from a physical model of the ES complex (for which abundant data are available), to give an atomistic physicochemical mechanism directly relevant to the medically important ischemic condition.

Aficionados will recognize a similarity between our SQ_o.ISPH$^\bullet$ state and a state proposed 20 years ago by Link[92] as a well-populated intermediate in forward chemistry. Because no such state was seen in EPR at the time, it was assumed that the complex was EPR invisible because of *quenching* between spins. That model was abandoned because detailed examination of the heme b_H kinetics precluded the high occupancy suggested, but the protective function by occlusion from reaction with O_2 that Link also suggested is now perhaps found in a complex with the EPR signal *enhanced* by spin sharing, formed only when protection is needed.

The Enzyme–Product Complex. The final EP complex after oxidation of the SQ (with Q.ISPH$^\bullet$) has not previously been modeled in any detail. However, it is a sensible starting state for characterization of native occupancies, since the complex is thermodynamically stable. It also results in perturbation of the g = 1.800 EPR spectrum of Q.ISPH$^\bullet$. Characterization of this state and its occupancy has engendered a substantial literature,[21,26,27,29,93,94] showing the thermodynamic forces associated with formation of the complex in wild-type and mutant strains.

Simulation of the Q_i-Site Reaction. The more stable model of the bc_1 complex studied by the Róg group,[35,36] with cardiolipin in the interfacial cavity and associated with each Q_i-site, allowed them to populate a series of model states for the reaction at the Q_i-site. The Q_i-site mechanism discussed was similar in outline to a previous model suggested by Kolling et al.[95] based on EPR/ESEEM studies, in which they pointed out the need for different patterns of H-bonding from the likely ligands (His-202, Asp-229, and Ser-206 in yeast or chicken; His-217, Asp-252, and Asn-221 in *Rhodobacter*), for the different states of the mechanism, site empty or with waters, or with Q, $Q^{\bullet-}$, or QH_2 bound. Their discussion[35,96] was in the context of crystallographic models from mitochondrial complexes in which the pattern of H-bonding showed several variants. These have provided information on the liganding of the Q_i-site occupant, but the possibility of radiative reduction in the X-ray beam left some uncertainty as to the redox state of the quinone species in the crystallographic models. However, in EPR studies,[90,97,98] the occupant is unequivocally semiquinone, and the data therefore more secure. The recent application of MD/QC approaches to the Q_i-site mechanism has provided new detail, and in particular has focused attention on the role of cardiolipin in facilitating access of protons to the reaction site, as originally proposed by Lange et al.[33] for the yeast bc_1 complex. The simulation was constructed using the *Rb. capsulatus* complex, in which the lipid constitution was based on the mitochondrial membrane that included cardiolipin in the lipid complement. In this model, binding sites equivalent to those observed in the yeast complex were spontaneously populated. Their simulation therefore provides a nice model (apart from obvious differences in protein sequence) for the important mitochondrial reaction, and with some interesting chemical insight in which a specific role of cardiolipin is discussed in detail. However, Kuleta et al.[96] recognized from their own and previous work[76,95,99−103] on strains mutated at the site that some plasticity in proton exchange pathways must be recognized. We would suggest that some caution should be observed in application of the Postila et al. model to the *Rb. sphaeroides* bc_1 complex. The suggested role for cardiolipin would require specific interaction with the protein, and might in turn be taken as indicating a specific functional requirement for cardiolipin. The crystallographic models available for the *Rb. sphaeroides* complex include some lipids but not cardiolipin. The structures are of good resolution (2.4 Å), so electron densities at sites stabilized by specific binding might have been expected to allow modeling of structure.

The question of specificity for cardiolipin as a function of the *Rb. sphaeroides* bc_1 complex has been addressed in the context of a similar argument made for a role for cardiolipin in cytochrome oxidase function, and investigated experimentally in this system. Since the complex turns over rapidly in the absence of cardiolipin, there can be no such requirement.[41] This interesting case and the outcome of our own simulation of the Q_i-site complex are discussed in detail in the Supporting Information.

DOI: 10.1021/acs.jpcb.6b10524
J. Phys. Chem. B 2017, 121, 3701−3717

Role of Asn-221 in the Two-Electron Gate Mechanism. One of the differences between mitochondrial and bacterial Q_i-sites is in the third potential ligand to the quinone occupants; Ser-206 is replaced by Asn-221. Mutation of the latter (N211 changed to T, H, I, S, P, D) was used to explore its role in the *Rb. sphaeroides* system. In N221 mutants, the reduction of heme b_H occurs at wild-type rates, but oxidation is slowed, in some cases dramatically. This inhibition was substantial even in the N221S strain (as in mitochondrial complexes). Earlier results had suggested that mutation to proline (N221P) had little effect on function, interpreted as showing that H-bonding could not play a significant role.[3,90] However, in later work, we found that frozen stocks of this strain when grown photosynthetically reverted to wild-type, and we could grow no authentic mutants without reversion.[98] Contrary to our previous suggestion, we have now concluded that the N221P mutation was nonfunctional, and that, since other mutant strains all showed an inhibited rate of electron transfer to the Q_i-site, a H-bonding function at this residue was essential. However, although inhibition was marked in N211I, with a nonpolar side chain, some mutants with polar side chains (N211D, H) showed similar inhibition, so other factors must be considered. Involvement of N211 in several H-bonding functions to the Q_i-site occupants was included in the Postila et al.[35] model. This residue is also within H-bonding distance of other side chains of the N-side structure, forming a potential proton-conducting network connecting the volume in which the H-bond between the Q_i-site occupant and His-217 is formed, the polar head groups of the void-filling PGs, and the N-phase waters (Figure SI-1, Supporting Information). It is perhaps also noteworthy that the isoprene tails of the ubiquinones interact extensively with the tails of the void-filling lipids.

Involvement of N221, and K251/D252, in H-bonded networks connecting to the heme b_L propionates brings into the discussion the features of the Q_i-site mechanism associated with the thermodynamic coupling between heme b_H and SQ_i.[100,104−106] With the Q_o-site blocked by myxothiazol and with heme b_H initially oxidized, introduction of QH_2 to the previously oxidized Q-pool (by redox titration, by generation on activation of reaction center turnover, or by addition of ascorbate as reductant) leads to generation of SQ_i and to reduction of heme b_H. In redox titrations, this is seen as "cyt *b*-150", a fraction of heme b_H titrating with an anomalously high potential ($E_{m,7} \sim 150$ mV).

$$QH_2 + [\text{vacant}].\text{ferriheme } b_H \rightleftharpoons [Q^{\bullet -}](H^+).\text{ferroheme } b_H + H^+$$

The reaction represents the reverse of the second step of the two-electron gate. Addition of antimycin induces a reversal of this reaction ("antimycin-induced oxidation of cyt *b*-150"), pulling the reaction to the left by binding to the vacant Q_i-site. Although no fully satisfactory treatment of the two-electron gate at the Q_i-site is yet available, the pH dependence of formation of SQ_i indicates the importance of coupling to protonation of groups other than the SQ itself, which has the characteristics of the anionic form. The interest in N221 mutants comes from the observation that in many strains the mutation changes the redox properties of the heme (most dramatically in N211I) but only in the presence of antimycin.[3] Although these aspects were not discussed by Postila et al.,[35] there can be little doubt that coordination between the redox states of the Q_i-site occupant and heme b_H is important to the mechanism. The most obvious channel for equilibration between the heme, quinone species in the site, and the *N*-side aqueous phase would be through the "bent" propionate (see the Supporting Information). However, the reduction of Q to QH_2 takes a proton at each end; it seems likely from the behavior of the N221 mutants that the H-bonded network linking quinone species to H217 and N221 is important in equilibration of the other proton.

Problems Immediately Accessible to Study Using the New Model. Now that our model is constructed and tested, simple MD simulations can access important problems. In addition to exploring Q-site binding, our initial efforts will address these "low hanging fruits".

a. Dynamics of Water Chains Associated with H^+ Transfer. Previously studies of water chains populated on MD equilibration in the bc_1 complex were of prime importance in formulating our current Q_o-site mechanism.[37,83] A proton channel could be traced from E295 (as proton acceptor from SQ_o) to the P-phase water, which included Y147, and linked to the heme b_L propionates. More recently, we have examined these in more detail,[4] and have looked at their stability on *in silico* mutagenesis. MD simulation of N279 mutants showed a broken continuity, thereby explaining the observed inhibition and validating the conjectural role of this residue. In the mechanism proposed, the properties of the intermediate state are determined by the redox state of heme b_L, and a coupling with the protonation of E295 through dynamics of the water chains. Similar problems can be addressed at the Q_i-site. The general approach of exploring the role of specific residues though *in silico* mutagenesis comparison to experimental outcomes will be continued, and extended to other water chains, residues likely to stabilize them.

b. The Marcus Reorganization Energy Explored through MD. Dielectric response to redox change and dielectric compensation on electron and proton transfer are critical components of the reorganization energy, λ, at the heart of theory of electron transfer, but values are often simply guessed. In the classical Marcus approach, the term to which λ makes the main contribution represents the activation free energy, describing the probability of reaching the activation barrier for forward chemistry. For biochemical reactions in the ms range, this is a thermal equilibrium state; the question of a time range for different components of λ is not applicable, although it would obviously be pertinent to photochemically driven reactions.[107,108] Matyushov has introduced a computational approach to estimation of local dielectric response from MD trajectories, which also addresses the time scales over which these operate. The approach was recently applied by Martin et al. in studies of the bc_1 complex.[38,109] Unfortunately, in the treatment of the Q_o-site reaction, they failed to take account of the coupled transfer of electron and proton in the first electron transfer, which determines that the process is electroneutral. The calculation of dielectric response for a simple electron transfer (with full electrostatic impact) was therefore inappropriate to the actual process. In using our new MD model, we will extend this work to calculation of dielectric response to redox changes on electron transfer, taking account of electrostatic imbalance only when charges separate (for example, in the second but not the first e-transfer from QH_2). A similar approach can be applied to transfer of H^+ through H-bonded pathways, which usually contain water chains to provide a Grotthuss proton-conducting channel. Both stabilization and dielectric compensation can be achieved via polarity

DOI: 10.1021/acs.jpcb.6b10524
J. Phys. Chem. B 2017, 121, 3701−3717

along the chain, but no detailed study of H^+ transfer in the bc_1 complex system has explored these roles.

c. Testing the Spring-Loaded Model for Control of the Q_o-Site Reaction. The counteracting forces involved in control of the Q_o-site reaction are determined by conformation changes of the ISP tether span, and by binding forces involving the catalytic interface with cyt *b* and the Q_o-site occupant. Mutations of the tether region interfere with the former, and mutations of interfacial residues in the ISP head (the mobile cluster binding domain) interfere with the latter. The effects of these mutations lead to changes in the balance between forces, and have been explored though thermodynamic and kinetic measurements on strains with mutations at these locations.[19,20,25−27,110] To understand the atomistic underpinnings of these changes, we can determine the energetics and examine the consequence of *in silico* mutagenesis on MD behaviors, with pathways explored through umbrella sampling of intermediate states.

d. Mobility of Q, QH_2, $QH^\bullet$, and $Q^{\bullet-}$ in the Quinone-Processing Sites. Exchange of QH_2 and Q at catalytic sites involves a diffusional path, often through a significant distance. From simulation of ES complex formation at the Q_o-site, QH_2 can diffuse rapidly in the entrance channel (as fast as ∼4 Å/ns, Figure 5B). In facilitating the second electron transfer of the bifurcated reaction, $Q^{\bullet-}$ likely moves 5−7 Å in the Q_o-site. The rate for QH_2 diffusion provides an estimate of the diffusional rate of SQ_o. No previous studies have reported how fast these diffusional processes are, or explored the constraints on rate from spontaneous reorganization of local structure at the site. The $Q^{\bullet-}$ movement could be gated by Coulombic effects linked to the redox status of heme b_L, which we have previously suggested might be important in control of bypass reactions.[2] These features will be explored by MD simulations and umbrella sampling of energy profiles at points along the putative path.

e. Exploration of the Effects of in Silico Mutagenesis. Molecular engineering has been used extensively to probe features of the mechanism, but few of the mutant strains have been structurally characterized. Interpretation of effects of mutagenesis has therefore often been conjectural. It is straightforward to implement such mutations *in silico*, and to use MD to explore possible reconfiguration of the local protein structure. Mutation can often have longer-range effects, especially if changes in polarity or charge are involved, but MD simulation is driven by calculation of local forces, and can therefore be readily adapted to calculation of energy changes and local reconfiguration on mutation. Such approaches can provide useful insights to underlying mechanistic changes (see also section c above).

■ ASSOCIATED CONTENT

Supporting Information

The Supporting Information is available free of charge on the ACS Publications website at DOI: 10.1021/acs.jpcb.6b10524.

Further data on the configuration of the ES-complex at the Q_i-site, and discussion of the role of cardiolipin in the Q_i-site reactions, and of a spin-coupled SQ.ISPH complex generated on long-term incubation under conditions in which heme b_L remains oxidized (PDF)

■ AUTHOR INFORMATION

Corresponding Author

*Address: 419 Roger Adams Lab, 600 S. Mathews Ave, Urbana, IL 61801. Phone: (217) 333-2043. E-mail: crofts@illinois.edu.

ORCID

Antony R. Crofts: 0000-0003-3211-1349

Paul J. A. Kenis: 0000-0001-7348-0381

Present Address

⊥R.L.B.: Department of Biochemistry & Molecular Biology, Michigan State University, 603 Wilson Road, East Lansing, MI 48824.

Author Contributions

The manuscript was written through contributions of all authors. All authors have given approval to the final version of the manuscript.

Funding

Pulsed EPR studies were supported in part by Grant DE-FG02-08ER15960 from Chemical Sciences, Geosciences and Biosciences Division, Office of Basic Energy Sciences, Office of Sciences, US DOE (S.A.D. and A.R.C.), and NCRR/NIH Grants S10-RR15878 and S10-RR025438 for pulsed EPR instrumentation. Computational resources were provided through an XSEDE startup grant MCB150083 and XSEDE Research Request MCB160130 to A.R.C.

Notes

The authors declare no competing financial interest.

■ ACKNOWLEDGMENTS

This paper is dedicated to the memory of Klaus Schulten, a giant in his field, and our collaborator on several earlier exercises in molecular dynamic and quantum chemical simulations of aspects of the bc_1 complex mechanism. These included the first such work, in collaboration with Sergei Izrailev and Ed Berry, analyzing the domain movement of the iron−sulfur protein, which also revealed water chains that were likely associated with H^+ exit from the Q_o-site reaction. Our most recent effort was in collaboration with Angela Barragan and Ilia Solov'yov, on detailed analysis of possible models for the ES complex, which provided the inspiration for the present work. I hereby acknowledge by deep indebtedness to all of these authors for taking on an ignorant (and sometimes truculent) biologist, and stimulating a recent flood of papers from other laboratories on this interesting topic.

■ REFERENCES

(1) Crofts, A. R. Proton-coupled electron transfer at the Q_o-site of the bc_1 complex controls the rate of ubihydroquinone oxidation. *Biochim. Biophys. Acta, Bioenerg.* **2004**, *1655*, 77−92.

(2) Crofts, A. R.; Lhee, S.; Crofts, S. B.; Cheng, J.; Rose, S. Proton pumping in the bc_1 complex: A new gating mechanism that prevents short circuits. *Biochim. Biophys. Acta, Bioenerg.* **2006**, *1757*, 1019−1034.

(3) Crofts, A. R.; Holland, J. T.; Victoria, D.; Kolling, D. R.; Dikanov, S. A.; Gilbreth, R.; Lhee, S.; Kuras, R.; Kuras, M. G. The Q-cycle reviewed: How well does a monomeric mechanism of the bc_1 complex account for the function of a dimeric complex? *Biochim. Biophys. Acta, Bioenerg.* **2008**, *1777* (7−8), 1001−19.

(4) Crofts, A. R.; Hong, S.; Wilson, C.; Burton, R.; Victoria, D.; Harrison, C.; Schulten, K. The mechanism of ubihydroquinone oxidation at the Q_o-site of the cytochrome bc_1 complex. *Biochim. Biophys. Acta, Bioenerg.* **2013**, *1827*, 1362−1377.

(5) Crofts, A. R.; Shinkarev, V. P.; Kolling, D. R. J.; Hong, S. The modified Q-cycle explains the apparent mismatch between the kinetics

DOI: 10.1021/acs.jpcb.6b10524
J. Phys. Chem. B 2017, 121, 3701−3717

of reduction of cytochromes c_1 and b_H in the bc_1 complex. *J. Biol. Chem.* **2003**, *278*, 36191−36201.
(6) Victoria, D.; Burton, R.; Crofts, A. R. Role of the -PEWY-glutamate in catalysis at the Q_o-site of the cyt bc_1 complex. *Biochim. Biophys. Acta, Bioenerg.* **2013**, *1827*, 365−386.
(7) Lhee, S.; Kolling, D. R.; Nair, S. K.; Dikanov, S. A.; Crofts, A. R. Modifications of protein environment of the [2Fe-2S] cluster of the bc_1 complex: effects on the biophysical properties of the Rieske iron-sulfur protein and on the kinetics of the complex. *J. Biol. Chem.* **2010**, *285* (12), 9233−48.
(8) Barragan, A. M.; Crofts, A. R.; Schulten, K.; Solov'yov, I. A. Identication of ubiquinol binding motifs at the Q_o-site of the cytochrome bc_1 complex. *J. Phys. Chem. B* **2015**, *119* (2), 433−47.
(9) Berry, E. A.; De Bari, H.; Huang, L.-S. Unanswered questions about the structure of cytochrome bc_1 complexes. *Biochim. Biophys. Acta, Bioenerg.* **2013**, *1827*, 1258−1277.
(10) Esser, L.; Quinn, B.; Li, Y.-F.; Zhang, M.; Elberry, M.; Yu, L.; Yu, C.-A.; Xia, D. Crystallographic studies of quinol oxidation site inhibitors: A modified classification of Inhibitors for the cytochrome bc_1 complex. *J. Mol. Biol.* **2004**, *341*, 281−302.
(11) Kim, H.; Xia, D.; Yu, C. A.; Xia, J. Z.; Kachurin, A. M.; Zhang, L.; Yu, L.; Deisenhofer, J. Inhibitor binding changes domain mobility in the iron-sulfur protein of the mitochondrial bc_1 complex from bovine heart. *Proc. Natl. Acad. Sci. U. S. A.* **1998**, *95*, 8026−8033.
(12) Xia, D.; Esser, L.; Tang, W.-K.; Zhou, F.; Zhou, Y.; Yu, L.; Yu, C.-A.; Meunier, B. Structural analysis of cytochrome bc_1 complexes: Implications to the mechanism of function. *Biochim. Biophys. Acta, Bioenerg.* **2013**, *1827* (11−12), 1278−1294.
(13) Xia, D.; Yu, C.-A.; Kim, H.; Xia, J.-Z.; Kachurin, A. M.; Zhang, L.; Yu, L.; Deisenhofer, J. Crystal Structure of the Cytochrome bc_1 Complex from Bovine Heart Mitochondria. *Science* **1997**, *277*, 60−66.
(14) Zhang, Z.; Huang, L.-S.; Shulmeister, V. M.; Chi, Y.-I.; Kim, K.-K.; Hung, L.-W.; Crofts, A. R.; Berry, E. A.; Kim, S.-H. Electron transfer by domain movement in cytochrome bc_1. *Nature (London, U. K.)* **1998**, *392* (6677), 677−684.
(15) Tso, S.-C.; Shenoy, S. K.; Quinn, B. N.; Yu, L. Subunit IV of cytochrome bc_1 complex from *Rhodobacter sphaeroides*: localization of regions essential for interaction with the three subunit complex. *J. Biol. Chem.* **2000**, *275* (20), 15287−15294.
(16) Andrews, K. M.; Crofts, A. R.; Gennis, R. B. Large scale purification and characterization of a highly active four-subunit cytochrome bc_1 complex from *Rb. sphaeroides*. *Biochemistry* **1990**, *29*, 2645−2651.
(17) Berry, E. A.; Lee, D.-W.; Huang, L.-S.; Daldal, F. Structural and mutational studies of the Cytochrome bc_1 Complex. In *The Purple Phototrophic Bacteria*; Hunter, C. N., Daldal, F., Thurnauer, M. C., Beatty, J. T., Eds.; Springer: Dordrecht, The Netherlands, 2009.
(18) Hunte, C.; Solmaz, S.; Palsdóttir, H.; Wenz, T. A structural perspective on mechanism and function of the cytochrome bc_1 complex. *Bioenergetics* **2008**, *45*, 253−278.
(19) Jafari, G.; Wasko, B. M.; Tong, A.; Schurman, N.; Dong, C.; Li, Z.; Peters, R.; Kayser, E.-B.; Pitt, J. N.; Morgan, P. G.; Sedensky, M. M.; Crofts, A. R.; Kaeberlein, M. Tether mutations that restore function and suppress pleiotropic phenotypes of the *C. elegans isp-1(qm150)* Rieske iron-sulfur protein. *Proc. Natl. Acad. Sci. U. S. A.* **2015**, *112* (45), E6148−E6157.
(20) Jafari, G.; Wasko, B. M.; Kaeberlein, M.; Crofts, A. R. New functional and biophysical insights into the mitochondrial Rieske iron-sulfur protein from genetic suppressor analysis in *C. elegans*. *Worm* **2016**, *5* (2), e1174803.
(21) Crofts, A. R.; Barquera, B.; Gennis, R. B.; Kuras, R.; Guergova-Kuras, M.; Berry, E. A. Mechanism of ubiquinol oxidation by the bc_1 complex: the different domains of the quinol binding pocket, and their role in mechanism, and the binding of inhibitors. *Biochemistry* **1999**, *38*, 15807−15826.
(22) Crofts, A. R.; Guergova-Kuras, M.; Huang, L.-S.; Kuras, R.; Zhang, Z.; Berry, E. A. The mechanism of ubiquinol oxidation by the bc_1 complex: the role of the iron sulfur protein, and its mobility. *Biochemistry* **1999**, *38*, 15791−15806.
(23) Cape, J. L.; Bowman, M. K.; Kramer, D. M. A semiquinone intermediate generated at the Q_o site of the cytochrome bc_1 complex: Importance for the Q-cycle and superoxide production. *Proc. Natl. Acad. Sci. U. S. A.* **2007**, *104*, 7887−7892.
(24) Burton, R. L. Q_o site of the bc_1 complex; unlocking the gate of the electron transport chain. Ph.D. Dissertation, University of Illinois at Urbana-Champaign, Urbana, IL, 2015.
(25) Crofts, A. R.; Shinkarev, V. P.; Dikanov, S. A.; Samoilova, R. I.; Kolling, D. Interactions of quinone with the iron-sulfur protein of the bc_1 complex: is the mechanism spring-loaded? *Biochim. Biophys. Acta, Bioenerg.* **2002**, *1555* (1−3), 48−53.
(26) Darrouzet, E.; Valkova-Valchanova, M.; Daldal, F. The [2Fe-2S] cluster E_m as an indicator of the iron-sulfur subunit position in the ubihydroquinone oxidation site of the cytochrome bc_1 complex. *J. Biol. Chem.* **2002**, *277*, 3464−3470.
(27) Darrouzet, E.; Daldal, F. Protein-protein interactions between cytochrome *b* and the Fe-S protein subunits during QH_2 oxidation and large-scale domain movement in the bc_1 complex. *Biochemistry* **2003**, *42*, 1499−1507.
(28) Darrouzet, E.; Moser, C. C.; Dutton, P. L.; Daldal, F. Large scale domain movement in cytochrome bc_1: a new device for electron transfer in proteins. *Trends Biochem. Sci.* **2001**, *26* (7), 445−451.
(29) Darrouzet, E.; Valkova-Valchanova, M.; Daldal, F. Probing the role of the Fe-S rubunit hinge region during Q_o site catalysis in *Rhodobacter capsulatus* bc_1 complex. *Biochemistry* **2000**, *39*, 15475−15483.
(30) Crofts, A. R.; Hong, S.; Zhang, Z.; Berry, E. A. Physicochemical aspects of the movement of the Rieske iron sulfur protein during quinol oxidation by the bc_1 complex. *Biochemistry* **1999**, *38*, 15827−15839.
(31) Crofts, A. R. The Q-cycle, - a personal perspective. *Photosynth. Res.* **2004**, *80*, 223−243.
(32) Crofts, A. R.; Guergova-Kuras, M.; Ugulava, N.; Kuras, R.; Hong, S. Proton processing at the Q_o-site of the bc_1 complex of *Rhodobacter sphaeroides*. In *Proc. XIIth Congress of Photosynthesis Research*, Brisbane, Australia, **2002**; p 6.
(33) Lange, C.; Nett, J. H.; Trumpower, B. L.; Hunte, C. Specific roles of protein-phospholipid interactions in the yeast cytochrome bc_1 complex. *EMBO J.* **2001**, *20*, 6591−6600.
(34) Solmaz, S. R. N.; Hunte, C. Structure of complex III with bound cytochrome *c* in reduced state and definition of a minimal core interface for electron transfer. *J. Biol. Chem.* **2008**, *283* (25), 17542−17549.
(35) Postila, P. A.; Kaszuba, K.; Kuleta, P.; Vattulainen, I.; Sarewicz, M.; Osyczka, A.; Róg, T. Atomistic determinants of co-enzyme Q reduction at the Q_i-site of the cytochrome bc_1 complex. *Sci. Rep.* **2016**, *6*, 33607.
(36) Pöyry, S.; Cramariuc, O.; Postila, P. A.; Kaszuba, K.; Sarewicz, M.; Osyczka, A.; Vattulainen, I.; Róg, T. Atomistic simulations indicate cardiolipin to have an integral role in the structure of the cytochrome bc_1 complex. *Biochim. Biophys. Acta, Bioenerg.* **2013**, *1827*, 769−778.
(37) Izrailev, S.; Crofts, A. R.; Berry, E. A.; Schulten, K. Steered molecular dynamics simulation of the Rieske subunit motion in the cytochrome bc_1 complex. *Biophys. J.* **1999**, *77* (4), 1753−1768.
(38) Martin, D. R.; LeBard, D. N.; Matyushov, D. V. Coulomb soup of bioenergetics: Electron transfer in a bacterial bc_1 complex. *J. Phys. Chem. Lett.* **2013**, *4*, 3602−3606.
(39) Postila, P. A.; Kaszuba, K.; Sarewicz, M.; Osyczka, A.; Vattulainen, I.; Róg, T. Key role of water in proton transfer at the Q_o-site of the cytochrome bc_1 complex predicted by atomistic molecular dynamics simulations. *Biochim. Biophys. Acta, Bioenerg.* **2013**, *1827*, 761−768.
(40) Benning, C.; Huang, Z. H.; Gage, D. A. Accumulation of a novel glycolipid and a betaine lipid in cells of *Rhodobacter sphaeroides* grown under phosphate limitation. *Arch. Biochem. Biophys.* **1995**, *317* (1), 103−111.
(41) Zhang, X.; Hiser, C.; Tamot, B.; Benning, C.; Reid, G. E.; Ferguson-Miller, S. M. Combined genetic and metabolic manipulation of lipids in *Rhodobacter sphaeroides* reveals non-phospholipid

DOI: 10.1021/acs.jpcb.6b10524
J. Phys. Chem. B 2017, 121, 3701−3717

substitutions in fully active cytochrome *c* oxidase. *Biochemistry* **2011**, *50* (19), 3891−3902.
(42) Baccarini-Melandri, A.; Gabellini, N.; Melandri, B. A.; Jones, K. R.; Rutherford, A. W.; Crofts, A. R.; Hurt, E. Differential extraction and structural specificity of specialized ubiquinone molecules in secondary electron transfer in chromatophores from *Rps. sphaeroides* GA. *Arch. Biochem. Biophys.* **1982**, *216* (2), 566−580.
(43) Baccarini-Melandri, A.; Melandri, B. A. A role for ubiquinone-10 in the *b*-c_2 segment of the photosynthetic bacterial electron transport chain. *FEBS Lett.* **1977**, *80* (2), 459−464.
(44) Takamiya, K.-I.; Dutton, P. L. Ubiquinone in *Rhodopseudomonas sphaeroides*. Some thermodynamic properties. *Biochim. Biophys. Acta, Bioenerg.* **1979**, *546* (1), 1−16.
(45) Phillips, J. C.; Braun, R.; Wang, W.; Gumbart, J.; Tajkhorshid, E.; Villa, E.; Chipot, C.; Skeel, R. D.; Kalé, L.; Schulten, K. Scalable molecular dynamics with NAMD. *J. Comput. Chem.* **2005**, *26* (16), 1781−1802.
(46) Klauda, J. B.; Venable, R. M.; Freites, J. A.; O'Connor, J. W.; Tobias, D. J.; Mondragon-Ramirez, C.; Vorobyov, I.; MacKerell, A. D., Jr.; Pastor, R. W. Update of the CHARMM all-atom additive force field for lipids: Validation on six lipid types. *J. Phys. Chem. B* **2010**, *114*, 7830−7843.
(47) MacKerell, A. D., Jr.; Feig, M.; Brooks, C. L., III Extending the treatment of backbone energetics in protein force fields: Limitations of gas-phase quantum mechanics in reproducing protein conformational distributions in molecular dynamics simulations. *J. Comput. Chem.* **2004**, *25*, 1400−1415.
(48) Jorgensen, W. L.; Chandrasekhar, J.; Madura, J. D.; Impey, R. W.; Klein, M. L. Comparison of simple potential functions for simulating liquid water. *J. Chem. Phys.* **1983**, *79*, 926−935.
(49) Martinetz, T.; Schulten, K. Topology representing networks. *Neural Networks* **1994**, *7*, 507−522.
(50) Feller, S. E.; Zhang, Y.; Pastor, R. W.; Brooks, B. R. Constant pressure molecular dynamics simulation: The Langevin piston method. *J. Chem. Phys.* **1995**, *103*, 4613−4621.
(51) Darden, T.; York, D.; Pedersen, L. G. Particle mesh Ewald: An *N*.log(*N*) method for Ewald sums in large systems. *J. Chem. Phys.* **1993**, *98*, 10089−10092.
(52) Torrie, G. M.; Valleau, J. P. Nonphysical sampling distributions in Monte Carlo free-energy estimation: Umbrella sampling. *J. Comput. Phys.* **1977**, *23*, 187−199.
(53) Sugita, Y.; Kitao, A.; Okamoto, Y. Multidimensional replica-exchange method for free-energy calculations. *J. Chem. Phys.* **2000**, *113*, 6042−6051.
(54) Kumar, A.; Kothekar, V. Stereochemical aspects of interactions of DNA binding domain of human progesterone receptor with $d(AGGTCATGCT)_2$. *Indian J. Biochem. Biophys.* **1992**, *29*, 236−244.
(55) Souaille, M.; Roux, B. Extension to the weighted histogram analysis method: combining umbrella sampling with free energy calculations. *Comput. Phys. Commun.* **2001**, *135*, 40−57.
(56) Frenkel, D.; Smit, B. *Understanding Molecular Simulation From Algorithms to Applications*; Academic Press: San Diego, CA, 2002.
(57) Zhu, J.; Egawa, T.; Yeh, S. R.; Yu, L.; Yu, C.-A. Simultaneous reduction of iron-sulfur protein and cytochrome b_L during ubiquinol oxidation in cytochrome bc_1 complex. *Proc. Natl. Acad. Sci. U. S. A.* **2007**, *104*, 4864−9.
(58) Lin, Y.; Gerfen, G. J.; Rousseau, D. L.; Yeh, S.-R. Ultrafast microfluidic mixer and freeze-quenching device. *Anal. Chem.* **2003**, *75*, 5381−5386.
(59) Manzerova, J.; Krymov, V.; Gerfen, G. J. Investigating the intermediates in the reaction of ribonucleoside triphosphate reductase from *Lactobacillus leichmannii*: an application of HF EPR-RFQ technology. *J. Magn. Reson.* **2011**, *213*, 32−45.
(60) Li, Y.; Zhang, D.; Feng, X.; Xu, Y.; Liu, B. F. A microsecond microfluidic mixer for characterizing fast biochemical reactions. *Talanta* **2012**, *88*, 175−180.
(61) Appleyard, R. J.; Shuttleworth, W. A.; Evans, J. N. Time-resolved solid-state NMR spectroscopy of 5-enolpyruvylshikimate-3-phosphate synthase. *Biochemistry* **1994**, *33*, 6812−6821.
(62) Czapla, M.; Borek, A.; Sarewicz, M.; Osyczka, A. Enzymatic activities of isolated cytochrome bc_1-like complexes containing fused cytochrome *b* subunits with asymmetrically inactivated segments of electron transfer chains. *Biochemistry* **2012**, *51*, 829−835.
(63) Hong, S.; Victoria, D.; Crofts, A. R. Inter-monomer electron transfer is too slow to compete with monomeric turnover in bc_1 complex. *Biochim. Biophys. Acta, Bioenerg.* **2012**, *1817*, 1053−1062.
(64) Sarewicz, M.; Bujnowicz, Ł.; Bhaduri, S.; Singh, S. K.; Cramer, W. A.; Osyczka, A. Metastable radical state, nonreactive with oxygen, is inherent to catalysis by respiratory and photosynthetic cytochromes bc_1/b_6f. *Proc. Natl. Acad. Sci. U. S. A.* **2017**, *114*, 1323.
(65) Moser, C. C.; Keske, J. M.; Warncke, K.; Farid, R. S.; Dutton, P. L. Nature of biological electron transfer. *Nature* **1992**, *355* (6363), 796−802.
(66) Crofts, A. R.; Rose, S. Marcus treatment of endergonic reactions: a commentary. *Biochim. Biophys. Acta, Bioenerg.* **2007**, *1767* (10), 1228−32.
(67) Guergova-Kuras, M.; Kuras, R.; Ugulava, N.; Hadad, I.; Crofts, A. R. Specific mutagenesis of the Rieske iron sulfur protein in *Rhodobacter sphaeroides* shows that both thermodynamic gradient and the pK of the oxidized form determine the rate of quinol oxidation by the bc_1 complex. *Biochemistry* **2000**, *39*, 7436−7444.
(68) Ugulava, N. B.; Crofts, A. R. CD-monitored redox titration of the Rieske Fe-S protein of *Rhodobacter sphaeroides*: pH dependence of the mid-point potential in isolated bc_1 complex and in membranes. *FEBS Lett.* **1998**, *440*, 409−413.
(69) Crofts, A. R.; Guergova-Kuras, M.; Kuras, R.; Ugulava, N.; Li, J.; Hong, S. Proton-coupled electron transfer at the Q_o-site: what type of mechanism can account for the high activation barrier? *Biochim. Biophys. Acta, Bioenerg.* **2000**, *1459*, 456−466.
(70) Link, T. A. Two pK values of the oxidised 'Rieske' [2Fe-2S] cluster observed by CD spectroscopy. *Biochim. Biophys. Acta, Bioenerg.* **1994**, *1185*, 81−84.
(71) Zu, Y.; Couture, M. M.-J.; Kolling, D. R. J.; Crofts, A. R.; Eltis, L. D.; Fee, J. A.; Hirst, J. The reduction potentials of Rieske clusters: the importance of the coupling between oxidation state and histidine protonation state. *Biochemistry* **2003**, *42*, 12400−12408.
(72) Brandt, U.; Okun, J. G. Role of deprotonation events in ubihydroquinone: cytochrome *c* oxidoreductase from bovine heart and yeast mitochondria. *Biochemistry* **1997**, *36*, 11234−11240.
(73) Hong, S. J.; Ugulava, N.; Guergova-Kuras, M.; Crofts, A. R. The energy landscape for ubihydroquinone oxidation at the Q_o-site of the bc_1 complex in *Rhodobacter sphaeroides*. *J. Biol. Chem.* **1999**, *274*, 33931−33944.
(74) Hsueh, K.-L.; Westler, W. M.; Markley, J. L. NMR investigations of the Rieske protein from *Thermus thermophilus* support a coupled proton and electron transfer mechanism. *J. Am. Chem. Soc.* **2010**, *132*, 7908−7918.
(75) Roberts, J. A.; Kirby, J. P.; Wall, S. T.; Nocera, D. G. Electron transfer within ruthenium(II) polypyridyl-(salt bridge)-dimethylaniline acceptor-donor complexes. *Inorg. Chim. Acta* **1997**, *263*, 395−405.
(76) Saribas, A. S.; Ding, H.; Dutton, P. L.; Daldal, F. Tyrosine 147 of cytochrome *b* is required for efficient electron transfer at the ubihydroquinone oxidase site (Q_o) of the cytochrome bc_1 complex. *Biochemistry* **1995**, *34*, 16004−16012.
(77) Shimizu, M.; Katsuda, N.; Katsurada, T.; Mitani, M.; Yoshioka, Y. Mechanism on two-electron oxidation of ubiquinol at the Q_p site of cytochrome bc_1 complex: B3LYP study with broken symmetry. *J. Phys. Chem. B* **2008**, *112*, 15116−15126.
(78) Barragan, A. M.; Schulten, K.; Solov'yov, I. A. Mechanism of the primary charge transfer reaction in the cytochrome bc_1 complex. *J. Phys. Chem. B* **2016**, *120* (44), 11369−11380.
(79) Husen, P.; Solov'yov, I. A. Mutations at the Q_o site of the cytochrome bc_1 complex strongly affect oxygen binding. *J. Phys. Chem. B* **2016**, DOI: 10.1021/acs.jpcb.6b08226.
(80) Husen, P.; Solov'yov, I. A. Spontaneous binding of molecular oxygen at the Q_o-site of the bc_1 complex could stimulate superoxide formation. *J. Am. Chem. Soc.* **2016**, *138*, 12150−12158.

DOI: 10.1021/acs.jpcb.6b10524
J. Phys. Chem. B 2017, 121, 3701−3717

(81) Kolling, D. R.; Samoilova, R. I.; Shubin, A. A.; Crofts, A. R.; Dikanov, S. A. Proton environment of reduced Rieske iron-sulfur cluster probed by two-dimensional ESEEM spectroscopy. *J. Phys. Chem. A* **2009**, *113* (4), 653−67.
(82) Ullmann, G. M.; Noodleman, L.; Case, D. A. Density functional calculation of pK_a values and redox potentials in the bovine Rieske iron-sulfur protein. *J. Biol. Inorg. Chem.* **2002**, *7*, 632−639.
(83) Crofts, A. R.; Hong, S. J.; Ugulava, N.; Barquera, B.; Gennis, R.; Guergova-Kuras, M.; Berry, E. A. Pathways for proton release during ubihydroquinone oxidation by the bc_1 complex. *Proc. Natl. Acad. Sci. U. S. A.* **1999**, *96* (18), 10021−10026.
(84) Cukier, R. I. Quantum molecular dynamics simulation of proton transfer in cytochrome oxidase. *Biochim. Biophys. Acta, Bioenerg.* **2004**, *1656*, 189−202.
(85) Russell, N. J.; Harwood, J. L. Changes in the acyl lipid composition of photosynthetic bacteria grown under photosynthetic and non-photosynthetic conditions. *Biochem. J.* **1979**, *181*, 339−45.
(86) Crofts, A. R.; Meinhardt, S. W.; Jones, K. R.; Snozzi, M. The role of the quinone pool in the cyclic electron-transfer chain of *Rhodopseudomonas sphaeroides*: A modified Q-cycle mechanism. *Biochim. Biophys. Acta, Bioenerg.* **1983**, *723* (2), 202−218.
(87) Osyczka, A.; Moser, C. C.; Dutton, P. L. Fixing the Q-cycle. *Trends Biochem. Sci.* **2005**, *30*, 176−182.
(88) Crofts, A. R.; Wang, Z. How rapid are the internal reactions of the ubiquinol:cytochrome c_2 oxidoreductase? *Photosynth. Res.* **1989**, *22*, 69−87.
(89) Rich, P. R. The quinone chemistry of *bc* complexes. *Biochim. Biophys. Acta, Bioenerg.* **2004**, *1658*, 165−171.
(90) Dikanov, S. A.; Holland, J. T.; Endeward, B.; Kolling, D. R.; Samoilova, R. I.; Prisner, T. F.; Crofts, A. R. Hydrogen bonds between nitrogen donors and the semiquinone in the Q_i-site of the bc_1 complex. *J. Biol. Chem.* **2007**, *282* (35), 25831−41.
(91) Sarewicz, M.; Dutka, M.; Pintscher, S.; Osyczka, A. Triplet State of the Semiquinone−Rieske Cluster as an Intermediate of Electronic Bifurcation Catalyzed by Cytochrome bc_1. *Biochemistry* **2013**, *52* (37), 6388−6395.
(92) Link, T. A. The role of the ″Rieske″ iron sulfur protein in the hydroquinone oxidation (Q_p-) site of the cytochrome bc_1 complex: The ″proton-gated affinity change″ mechanism. *FEBS Lett.* **1997**, *412*, 257−264.
(93) Samoilova, R. I.; Kolling, D.; Uzawa, T.; Iwasaki, T.; Crofts, A. R.; Dikanov, S. A. The interaction of the Rieske iron sulfur protein with occupants of the Q_o-site of the bc_1 complex, probed by 1D and 2D Electron Spin Echo Envelope Modulation. *J. Biol. Chem.* **2002**, *277*, 4605−4608.
(94) Ding, H.; Robertson, D. E.; Daldal, F.; Dutton, P. L. Cytochrome bc_1 complex [2Fe-2S] cluster and its interaction with ubiquinone and ubihydroquinone at the Q_o site: a double-occupancy Q_o site model. *Biochemistry* **1992**, *31*, 3144−3158.
(95) Kolling, D. R. J.; Samoilova, R. I.; Holland, J. T.; Berry, E. A.; Dikanov, S. A.; Crofts, A. R. Exploration of ligands to the Q_i-site semiquinone in the bc_1 complex using high resolution EPR. *J. Biol. Chem.* **2003**, *278*, 39747−39754.
(96) Kuleta, P.; Sarewicz, M.; Postila, P.; Róg, T.; Osyczka, A. Identifying involvement of Lys251/Asp252 pair in electron transfer and associated proton transfer at the quinone reduction site of *Rhodobacter capsulatus* cytochrome bc_1. *Biochim. Biophys. Acta, Bioenerg.* **2016**, *1857*, 1661−1668.
(97) Dikanov, S. A.; Samoilova, R. I.; Kolling, D. R. J.; Holland, J. T.; Crofts, A. R. Hydrogen bonds involved in binding the Q_i-site semiquinone in the bc_1 complex, identified through deuterium exchange using pulsed EPR. *J. Biol. Chem.* **2004**, *279*, 15814−15823.
(98) Hong, S.; de Almeida, W. B.; Taguchi, A. T.; Samoilova, R. I.; Gennis, R. B.; O'Malley, P. J.; Dikanov, S. A.; Crofts, A. R. The semiquinone at the Q_i site of the bc_1 complex explored using HYSCORE spectroscopy and specific isotopic labeling of ubiquinone in *Rhodobacter sphaeroides* via ^{13}C methionine and construction of a methionine auxotroph. *Biochemistry* **2014**, *53* (38), 6022−6031.
(99) Gray, K. A.; Dutton, P. L.; Daldal, F. Requirement of histidine-217 for ubiquinone reductase activity (Q_i-site) in the cytochrome-bc_1 complex. *Biochemistry* **1994**, *33*, 723−733.
(100) Hacker, B.; Barquera, B.; Crofts, A. R.; Gennis, R. B. Characterization of mutations in the cytochrome *b* subunit of the bc_1 complex of *Rhodobacter sphaeroides* that affect the quinone reductase site (Q_c). *Biochemistry* **1993**, *32*, 4403−4410.
(101) Hacker, B.; Barquera, B.; Gennis, R. B.; Crofts, A. R. Site-directed mutagenesis of arginine-114 and tryptophan-129 in the cytochrome *b* subunit of the bc_1 complex of *Rhodobacter sphaeroides*: two highly conserved residues predicted to be near the cytoplasmic surface of putative transmembrane helices B and C. *Biochemistry* **1994**, *33*, 13022−13031.
(102) Yun, C.-H.; Wang, Z.; Crofts, A. R.; Gennis, R. B. Examination of the functional roles of five highly conserved residues in the cytochrome *b* subunit of the *bc*1 complex of *Rhodobacter sphaeroides*. *J. Biol. Chem.* **1992**, *67*, 5901−5909.
(103) Brasseur, G.; Sami Saribas, A.; Daldal, F. A compilation of mutations located in the cytochrome *b* subunit of the bacterial and mitochondrial bc_1 complex. *Biochim. Biophys. Acta, Bioenerg.* **1996**, *1275*, 61−69.
(104) Crofts, A. R. The cytochrome bc_1 complex − function in the context of structure. *Annu. Rev. Physiol.* **2004**, *66*, 689−733.
(105) Meinhardt, S. W.; Crofts, A. R. A New Effect of Antimycin on the *b*-cytochromes of *Rps. sphaeroides*. In *Advances in Photosynthesis Research*; Sybesma, C., Ed.; Martinus Nijhoff/Dr. W. Junk Publishers: The Hague, The Netherlands, 1984; Vol. *1*, pp 649−652.
(106) Glaser, E. G.; Meinhardt, S. W.; Crofts, A. R. Reduction of cytochrome b-561 through the antimycin-sensitive site of the ubiquinol-cytochrome c_2 oxidoreductase complex of *Rhodopseudomonas sphaeroides*. *FEBS Lett.* **1984**, *178* (2), 336−342.
(107) Abbyad, P.; Childs, W.; Shi, X.; Boxer, S. G. Dynamic Stokes shift in green fluorescent protein variants. *Proc. Natl. Acad. Sci. U. S. A.* **2007**, *104* (51), 20189−20194.
(108) Matyushov, D. V. Protein electron transfer: Dynamics and statistics. *J. Chem. Phys.* **2013**, *139*, 025102−14.
(109) Martin, D. R.; Matyushov, D. V. Microsecond dynamics of the protein and water affect electron transfer in a bacterial bc_1 complex. *J. Chem. Phys.* **2015**, *142*, 161101−161104.
(110) Darrouzet, E.; Valkova-Valchanova, M.; Moser, C. C.; Dutton, P. L.; Daldal, F. Uncovering the [2Fe2S] domain movement in cytochrome bc_1 and its implications for energy conversion. *Proc. Natl. Acad. Sci. U. S. A.* **2000**, *97*, 4567−4572.
(111) Zhang, H.; Osyczka, A.; Dutton, P. L.; Moser, C. C. Exposing the complex III Q_o semiquinone radical. *Biochim. Biophys. Acta, Bioenerg.* **2007**, *1767*, 883−887.

DOI: 10.1021/acs.jpcb.6b10524
J. Phys. Chem. B 2017, 121, 3701−3717